THE ASTROPHYSICAL JOURNAL, 432:274–295, 1994 September 1

RESONANCE LINE POLARIZATION IN SPHERICAL ATMOSPHERES: PARTIAL REDISTRIBUTION EFFECTS STUDIED WITH THE DOMKE–HUBENY REDISTRIBUTION MATRIX

K. N. NAGENDRA
Indian Institute of Astrophysics, Bangalore 560 034, India
Received 1993 October 18; accepted 1994 March 1

ABSTRACT

The problem of resonance line polarization including collisional redistribution is studied using simple theoretical models. The medium is assumed to be a static finite spherical shell atmosphere. The purpose of this paper is to understand the behavior of line polarization when elastic and inelastic collisions cause frequency redistribution upon scattering. All the redistribution mechanisms that are astrophysically relevant are considered in a simple two-level atom picture. The dependence of resonance line polarization on physical parameters of the two-level atom formulation and on the collisional parameters is shown in detail. The Domke–Hubeny generalized collisional redistribution matrix for polarized radiation is employed in most of the examples shown in this paper. It is shown that different types of collisions that affect photon redistribution in both resonance and subordinate lines can be distinguished through the characteristic changes they produce in the intensity and linear polarization profiles. The simple asymptotic expressions of partial redistribution theory are shown to be useful in the interpretation of model intensity and polarization profiles.

Subject headings: line: formation — polarization — radiative transfer — stars: atmospheres

1. INTRODUCTION

Several aspects of line formation theory including polarization of radiation fields have been well explored in the past two decades. In an important article Rees & Murphy (1987) review the developments achieved in this area, and the future prospects. Since a detailed reference to earlier work is listed in that article, we refer only to the work done in recent years with specific emphasis on radiative transfer computations involving collisional redistribution of radiation during scattering. Saliba (1985) made a detailed study of the linear polarization in the solar Ca II K line in a realistic solar atmosphere. He included the effect of collisions in a partial frequency redistribution (PRD) model, according to the well-known method of Omont, Smith, & Cooper (1972) and Ballagh & Cooper (1977). His approach is practically very useful in modeling the observations of linear polarization of resonance lines in general. A similar kind of calculation is presented in McKenna (1984, 1985). The most general method to date to solve the transfer problems including collisions and weak magnetic fields is due to Faurobert-Scholl (1991, 1992, 1993 and references therein). In this important series of papers, she has included one of the most general collisional redistribution matrix for polarized radiation derived by Domke & Hubeny (1988). The presence of weak magnetic fields leads to the Hanle effect in the resonance lines. The general method developed earlier for the Hanle effect with PRD (Faurobert-Scholl 1991) is cleverly adopted to include the Domke–Hubeny redistribution matrix also (Faurobert-Scholl 1992, 1993). The collisional and radiative branching ratios are computed for a realistic solar atmosphere, and theoretical resonance line model profiles are fitted to the polarization observations of Stenflo, Baur, & Elmore (1980). Some aspects of polarized resonance line transfer using this matrix are also presented in Mohan Rao & Rangarajan (1993). In an important series of papers Landi degl'Innocenti, Bommier, & Sahal-Brechot (1990 and references therein to their series of papers) have developed a very general quantum electrodynamical formulation of the redistribution of polarized radiation in resonance lines, and methods to solve those equations. It is very important to note that Faurobert-Scholl (1991) has also established the "equivalence" of conventional approach (meaning the use of Hummer's redistribution functions along with independent coupling to statistical equilibrium equations, e.g., as described in Mihalas 1978) and the formulation of Landi degl'Innocenti and collaborators. It is useful to note that the calculations as presented in our paper are a limiting special case, when magnetic field strength in zero, of the general approaches developed in Faurobert-Scholl (1990, 1991, 1992) and Landi degl'Innocenti et al. (1990). The quantum mechanical collisional redistribution matrix for polarized radiation is derived by many authors (see Ballagh & Cooper 1977 and references therein to earlier work). Recently Domke & Hubeny (1988) and Streater, Cooper, & Rees (1988) have derived general redistribution matrices where certain simplifying approximations made in earlier work are relaxed. In all the references mentioned above, the line-forming region is assumed to be stratified in plane parallel layers. The PRD resonance line polarization problem in spherically symmetric atmospheres is presented in Nagendra (1988, 1989). This paper is devoted to exploring certain finer aspects of collisional redistribution on resonance and subordinate line polarization in spherical atmospheres. In § 2 we present the transfer equations. In §§ 2.1 and 2.2 we discuss the collisionless redistribution matrices and elementary redistribution functions, respectively. In § 2.3 we describe the Domke–Hubeny polarized redistribution matrix. In § 3 we discuss the results of our computation with the help of a large number of models.

2. GOVERNING EQUATIONS OF THE PROBLEM

2.1. *Polarized Line Transfer Equation*

The vector transfer equation in spherically symmetric (SS) media for polarized vector intensity $\boldsymbol{U} = 4\pi r^2 \boldsymbol{I}$, with $\boldsymbol{I} = (I\ Q)^T$ is written as

$$\mu \frac{\partial \boldsymbol{U}(x, \mu, r)}{\partial r} + \frac{1-\mu^2}{r} \frac{\partial \boldsymbol{U}(x, \mu, r)}{\partial \mu} = -\chi(x, \mu, r)\boldsymbol{U}(x, \mu, r) + \boldsymbol{\eta}(x, \mu, r) ,$$

in the conventional notation of two-level atom line transfer problems. The total absorption coefficient is given as

$$\chi(x, \mu, r) = \chi^L(r)\phi(x, \mu, r) + \chi^C(x, \mu, r) + \chi^e(x, \mu, r) .$$

The optical depth scale is $d\tau(r) = -\chi^L(r)dr$, defined in terms of averaged atomic absorption coefficient at the line center $\chi^L(r)$. The reduced frequency x is defined as $x = (\nu - \nu_0)/\Delta\nu_D$, where $\Delta\nu_D = (\nu_0/c)(2kT_e/M^a)^{1/2}$, where ν_0 is the line center frequency and M^a is the mass of radiating atom. The Doppler width $\Delta\nu_D$ is independent of optical depth since the medium is isothermal (T_e = constant). In the expression above, χ^C and χ^e are, respectively, the coefficients of continuous absorption and electron scattering ($\chi^e = N_e\sigma_e$, where σ_e is classical Thomson scattering coefficient and N_e the electron number density). The profile function is represented by a Voigt function

$$\phi(x) = \frac{1}{\sqrt{\pi}} H(a, x) ,$$

where damping parameter a is the ratio of total damping width Γ to the Doppler width $\Delta\nu_D$ (see eq. [54]). The emission coefficient vector $\boldsymbol{\eta}(x, \mu, r)$ in the transfer equation is defined as

$$\boldsymbol{\eta}(x, \mu, r) = \boldsymbol{\eta}^L(x, \mu, r) + \boldsymbol{\eta}^C(x, \mu, r) + \boldsymbol{\eta}^e(x, \mu, r) ,$$

in analogy with total absorption coefficient $\chi(x, \mu, r)$. The total "vector source function" is written as

$$\boldsymbol{S}_{\rm tot}(x, \mu, r) = \begin{bmatrix} S_I(x, \mu, r) \\ S_Q(x, \mu, r) \end{bmatrix} = \frac{\boldsymbol{\eta}(x, \mu, r)}{\chi(x, \mu, r)}$$

$$= \frac{\phi(x)\boldsymbol{S}^L(x, \mu, r) + \beta^C\boldsymbol{S}^C(r) + \beta^e\boldsymbol{S}^e(x, \mu, r)}{\phi(x) + \beta^C + \beta^e}$$

where the unpolarized continuum source vector $\boldsymbol{S}^C(r)$ is defined as

$$\boldsymbol{S}^C(r) = B(r)\mathbf{1} = B\mathbf{1}; \qquad \mathbf{1} = [1 \quad 0]^T .$$

The continuum absorption parameter $\beta^C = [\chi^C(r)/\chi^L(r)]$ is assumed to be frequency independent across the entire bandwidth of the line. The polarized line transfer equation given above is solved in spherically symmetric systems by giving boundary conditions at both the inner and outer boundaries. The Schuster boundary condition employed by us represents the photospheric boundary condition

$$\boldsymbol{U}(x, \mu, \tau = T^L) = [1 \quad 0]^T \qquad \text{and} \qquad \boldsymbol{U}(x, \mu, \tau = 0) = [0 \quad 0]^T ,$$

which is useful for optically thick (or semi-infinite) slabs or spherical shells. For simplicity, we have taken $B(\tau = T^L)$ to be frequency independent and angularly isotropic across the entire bandwidth of the line. The method of solution continues to be the same as in Nagendra (1988). The model parameterization is also the same as before. In the following sections, specific requirements of model parameterization are mentioned as and when required.

2.2. *Basic Concepts of Polarized Redistribution Matrices: The Collisionless Case*

In this section we give general expressions for line source vector, in the case where collisional redistribution is neglected. A two-level atom line source vector for this case is given by

$$\boldsymbol{S}^L(x, \mu, r) = \begin{bmatrix} S_I^L(x, \mu, r) \\ S_Q^L(x, \mu, r) \end{bmatrix} = \frac{(1-\epsilon)}{2\phi(x)} \int_{-\infty}^{+\infty} dx' \int_{-1}^{+1} \boldsymbol{R}(x, \mu, x', \mu')\boldsymbol{I}(x', \mu', r)d\mu' + \epsilon B\mathbf{1} , \tag{1}$$

where ϵ is the probability per scatter that a photon is destroyed by collisional de-excitation. The redistribution matrix $\boldsymbol{R}(x, \mu, x', \mu')$ can be approximated following the hybrid model

$$\boldsymbol{R}(x, \mu, x', \mu') = \boldsymbol{P}(\mu, \mu')R(x, x') \tag{2}$$

of Rees & Saliba (1982) which completely decouples angle and frequency dependence. The angular phase matrix is

$$\boldsymbol{P}(\mu, \mu') = \frac{1}{2\pi} \int_0^{2\pi} \boldsymbol{P}(\mu, \mu', \Delta)d\Delta ; \qquad \Delta = (\phi - \phi') , \tag{3}$$

in the conventional notation that direction (μ', ϕ') represents incoming ray and (μ, ϕ) the outgoing ray. Employing the expressions

for the phase matrix $\boldsymbol{P}(\mu, \mu', \Delta)$ in the $(I \quad Q)^T$ representation (cf. Chandrasekhar 1960),

$$\boldsymbol{P}(\mu, \mu', \Delta) = E_1 \begin{bmatrix} \frac{3}{4}(1 + \cos^2 \Theta) & \frac{3}{4}(1 + \cos^2 \Theta) - \frac{3}{2} + \frac{3}{2}(1 - \mu^2) \sin^2 \Delta \\ \frac{3}{4}(1 + \cos^2 \Theta) - \frac{3}{2} + \frac{3}{2}(1 - \mu'^2) \sin^2 \Delta & \frac{3}{4}(1 + \cos^2 \Theta) - \frac{3}{2}(\mu^2 + \mu'^2) \sin^2 \Delta \end{bmatrix} + (1 - E_1) \begin{pmatrix} 1 & 0 \\ 0 & 0 \end{pmatrix}, \tag{4}$$

where $(1 - E_1)$ measures the amount of atomic depolarization. Some remarks are made about the physical meaning of E_1 in the next section on redistribution functions. In all the computations presented in this paper we have taken $E_1 = 1$, excepting its indirect parameterization in the Domke–Hubeny redistribution matrix. In the equations that follow, we have assumed $E_1 = 1$. This does not cause any ambiguity. The scattering angle Θ in equation (4) is given by the expression

$$\cos \Theta = \mu\mu' + (1 - \mu^2)^{1/2}(1 - \mu'^2)^{1/2} \cos \Delta , \tag{5}$$

where $\mu = \cos \theta$, and $\mu' = \cos \theta'$ are the polar angles measured in the rest frame of the star (laboratory frame), in which all geometric and physical variables are measured. We now define three auxiliary functions that together constitute the redistribution matrix. They are

$$R^A(x, \mu, x', \mu') = R(x, x') \frac{1}{2\pi} \int_0^{2\pi} 1 \, d\Delta = R(x, x') , \tag{6a}$$

$$R^B(x, \mu, x', \mu') = R(x, x') \frac{1}{2\pi} \int_0^{2\pi} \frac{3}{4} (1 + \cos^2 \Theta) d\Delta$$

$$= R(x, x') \frac{3}{4} \left[1 + \mu^2\mu'^2 + \frac{1}{2} (1 - \mu^2)(1 - \mu'^2) \right], \tag{6b}$$

$$R^C(x, \mu, x', \mu') = R(x, x') \frac{1}{2\pi} \int_0^{2\pi} \sin^2 \Delta \, d\Delta = \frac{1}{2} R(x, x') . \tag{6c}$$

The redistribution matrix for the scattering of azimuthally symmetric, linearly polarized light in the base $(I \quad Q)^T$ is written as

$$\boldsymbol{R}(x, \mu, x', \mu') = \begin{bmatrix} R^{11}(x, \mu, x', \mu') & R^{12}(x, \mu, x', \mu') \\ R^{21}(x, \mu, x', \mu') & R^{22}(x, \mu, x', \mu') \end{bmatrix}. \tag{7}$$

In can be noticed that the first two expressions of equation (6) represent, respectively, the scalar isotropic scattering and Rayleigh scattering (or dipole scattering) redistribution functions, which are extensively employed in astrophysical line transfer problems. The individual matrix elements in equation (7) are given by

$$R^{11}(x, \mu, x', \mu') = R^B(x, \mu, x', \mu') , \tag{8a}$$

$$R^{12}(x, \mu, x', \mu') = R^B(x, \mu, x', \mu') - \tfrac{3}{2} R^A(x, \mu, x', \mu') + \tfrac{3}{2}(1 - \mu^2) R^C(x, \mu, x', \mu') , \tag{8b}$$

$$R^{21}(x, \mu, x', \mu') = R^B(x, \mu, x', \mu') - \tfrac{3}{2} R^A(x, \mu, x', \mu') + \tfrac{3}{2}(1 - \mu'^2) R^C(x, \mu, x', \mu') , \tag{8c}$$

$$R^{22}(x, \mu, x', \mu') = R^B(x, \mu, x', \mu') - \tfrac{3}{2}(\mu^2 + \mu'^2) R^C(x, \mu, x', \mu') . \tag{8d}$$

The normalization conditions to be satisfied in the finite angle and frequency representation of the redistribution functions are

$$\int_{-\infty}^{+\infty} dx' \tfrac{1}{2} \int_{-1}^{+1} R^{A,B}(x, \mu, x', \mu') d\mu' = \phi(x) , \tag{9}$$

for the isotropic and dipole scattering weighted redistribution functions. Further, the normalization condition

$$\int_{-\infty}^{+\infty} dx' \, \tfrac{1}{2} \int_{-1}^{+1} (1 - \mu'^2) R^C(x, \mu, x', \mu') d\mu' = \frac{\phi(x)}{3} \tag{10}$$

for the function $R^C(x, \mu, x', \mu')$ is derived by demanding that the polarization on scattering should vanish ($Q = 0$) in an isotropic diffuse radiation field. This requirement implies

$$\int_{-\infty}^{+\infty} dx' \tfrac{1}{2} \int_{-1}^{+1} R^{21}(x, \mu, x', \mu') d\mu' = 0 \tag{11}$$

in the equation (7) for redistribution matrix. The quantity $R(x, x')$ in equation (2) is the conventional angle-average laboratory frame redistribution function (see Mihalas 1978). In this paper we have studied some commonly used elementary atomic redistribution functions. Thus we can write $R(x, x')$ in a generic form as

$$R(x, x') = R_{i-A}(x, x') ; \qquad i = \text{II, III, V} \tag{12}$$

in Hummer's conventional notation. These functions can also be classified as mathematical redistribution functions (see Hubeny 1985b). Analogous to equation (1), we can write the electron scattering source function $S^e(x, \mu, r)$ as

$$\boldsymbol{S}^e(x, \mu, r) = \begin{bmatrix} S_I^e(x, \mu, r) \\ S_Q^e(x, \mu, r) \end{bmatrix} = \frac{1}{2} \int_{-\infty}^{+\infty} dx' \int_{-1}^{+1} \boldsymbol{R}^e(x, \mu, x', \mu') \boldsymbol{I}(x', \mu', r) d\mu' . \tag{13}$$

The electron scattering parameter $\beta^e = [\chi^e(r)/\chi^L(r)]$ gives the probability that a line photon is redistributed by scattering on an electron having a Maxwellian distribution of velocities. Since all the equations (2)–(11) hold exactly for the electron scattering also, we do not repeat them again. As in the case of atomic scattering, we have always selected $E_1^e = 1$ in this paper. The generic form of the redistribution function for electron scattering can be written as

$$R^e(x, x') = R^e_{j-A}(x, x') \; ; \qquad j = \text{CES, CRES} \tag{14a}$$

(see Mihalas, Kunasz, & Hummer 1975). The symbols CES and CRES stand for coherent electron scattering and complete redistribution in electron scattering, respectively. The explicit expressions for these choices are

$$R^e_{\text{CES}-A}(x, x') = \delta(x - x') \; ; \qquad \text{and} \qquad R^e_{\text{CRES}-A}(x, x') = 1 \; . \tag{14b}$$

Note that the profile function for electron scattering is constant (due to Thomson scattering cross section σ_e being constant).

2.3. *Elementary Redistribution Functions*

In this subsection, we mention some of the laboratory frame redistribution functions that are frequently used in astrophysical radiation transfer theory. An elegent description of physical nature of the functions $R_{i-A}(x, x')$, i = II, III along with plots of the corresponding emission coefficients can be found in Mihalas (1978). A complete description of $R_{i-A}(x, \mu, x', \mu')$, i = I, II, III, V can be found in Heinzel (1981) where the angle-dependent emission coefficients for different angles are also shown. The angle-averaged versions of the redistribution functions can be computed by a direct numerical integration of the corresponding angle-dependent functions (see Heinzel & Hubeny 1983; Hubeny & Heinzel 1984). It is important to note that redistribution functions $R_{i-A}(x, x')$, i = I, II, III derived by Hummer (1962) are special limiting cases of the more general function $R_{\text{V}-A}(x, x')$ derived by Heinzel (1981). The simplest function that can be employed as a line scattering mechanism is coherent scattering (CS) in the laboratory frame. But it represents a highly unrealistic and extreme case, and hence not useful in practice. It is defined as

$$R(x, x') = \delta(x - x')\phi(x') \; . \tag{15}$$

An extremely useful redistribution function that is widely used in literature is the complete noncoherent scattering in the laboratory frame (a situation opposite to that of CS). This function referred to as complete frequency redistribution (CRD) is given by

$$R(x, x') = \phi(x)\phi(x') \; . \tag{16}$$

CRD can be used as a good approximation to represent resonance scattering in resonance or subordinate lines. The type II $-$ A and type III $-$ A redistribution functions of Hummer are given in Mihalas (1978). The model profiles computed for $R_{\text{III}-A}$ redistribution function resemble the corresponding CRD profiles in certain frequency ranges in the line. However, unlike CRD function, $R_{\text{III}-A}(x, x')$ is employed mainly to represent the situation where collisional damping or collision-induced decay of the upper level is "dominant" over the radiative decay. The type V $-$ A redistribution function of Heinzel is obtained by an accurate angle averaging of the corresponding angle dependent function given by

$$R(x, x') = R_{\text{V}-A}(x, x') = 8\pi^2 \int_0^\pi R_{\text{V}}(x, x', \Theta) \sin \Theta \, d\Theta \; , \tag{17}$$

where the angle-dependent function is given by (Heinzel 1981):

$$R_{\text{V}-A}(x, x', \Theta) = \frac{1}{\pi \sin \Theta} \left\{ H\left[a_u \sec\left(\frac{\Theta}{2}\right), \frac{x + x'}{2} \sec\left(\frac{\Theta}{2}\right)\right] H\left[a_l \csc\left(\frac{\Theta}{2}\right), \frac{x - x'}{2} \csc\left(\frac{\Theta}{2}\right)\right] + E_{\text{V}}(x, x', \Theta)\right\} . \tag{18}$$

The correction function $E_{\text{V}}(x, x', \Theta)$ is given (after simplifications in the original expressions of Heinzel 1981) by

$$E_{\text{V}}(x, x', \Theta) = \frac{\sin(\Theta/2)}{\sqrt{\pi}} \text{Re} \int_0^\infty e^{-t^2 - 2a_{ul}t} \left[(\cos 2xt + \cos 2x't) \left\{ H\left[a_1, \frac{x + x'}{2} \sec\left(\frac{\Theta}{2}\right)\right] - H\left[a_2, \frac{x + x'}{2} \sec\left(\frac{\Theta}{2}\right)\right]\right\} \right.$$
$$\left. - (\sin 2xt + \sin 2x't) \left\{ K\left[a_1, \frac{x + x'}{2} \sec\left(\frac{\Theta}{2}\right)\right] - K\left[a_2, \frac{x + x'}{2} \sec\left(\frac{\Theta}{2}\right)\right]\right\}\right] dt \; , \tag{19}$$

where the composite damping parameters a_1 and a_2 are defined as

$$a_1 = a_u \sec(\Theta/2) + t \cos(\Theta/2) + a_l \sec(\Theta/2) \; ; \qquad \text{and} \qquad a_2 = a_u \sec(\Theta/2) + t \cos(\Theta/2) \; .$$

The H and K Voigt functions are the real and imaginary parts of the complex Dawson function defined as

$$D(\omega) = H(p, q) + iK(p, q) \; , \qquad \text{with} \qquad \omega = p - iq \; . \tag{20}$$

These H and K functions are computed using accurate methods given in Matta & Reichel (1971). The profile function to be employed when using $R_{\text{V}-A}(x, x')$ in the transfer equation, is computed from

$$\phi(x) = \frac{1}{\sqrt{\pi}} H(a_{ul}, x) = \int_{-\infty}^{+\infty} R_{\text{V}-A}(x, x') dx' \; , \tag{21}$$

with $a_{ul} = a_u + a_l$. The redistribution function $R_{\text{V}-A}(x, x')$ refers to the case of a subordinate line in which both the upper and lower

levels have finite widths caused by pure radiative damping of each level. This function represents partial noncoherence (fluorescence) in the atom's frame. This function is characterized by a joint probability of emission maxima in the wing and near the line center. The nature of core emission is like that of $R_{\mathrm{II}-A}(x, x')$ and the nature of wing emission is like that of $R_{\mathrm{III}-A}(x, x')$.

2.4. *Physical Redistribution Functions*

Since collisions of radiating atoms with neutral and charged perturbers is one of the basic causes of frequency redistribution, the name physical redistribution functions can be used to refer to those functions that explicitly include the effect of collisions. Such functions for spectral lines formed under partial frequency redistribution mechanism, are derived in Omont et al. (1972). They showed that, for resonance lines (no lower state broadening), the effects of collisional redistribution can be represented by taking a linear combination of elementary redistribution functions $R_{\mathrm{II}-A}(x, x')$ and $R_{\mathrm{III}-A}(x, x')$. The renormalized version of their collisional redistribution function is written as

$$R(x, x') = \Lambda R_{\mathrm{II}-A}(x, x') + (1 - \Lambda) R_{\mathrm{III}-A}(x, x') \, . \tag{22}$$

The renormalized branching ratio (also called coherence fraction) Λ is given by

$$\Lambda = \frac{\Gamma_R + \Gamma_I}{\Gamma_R + \Gamma_I + Q_E} \, , \tag{23}$$

where Γ_R, Γ_I, and Q_E are the radiative broadening rate, inelastic collision rate, and elastic collision rate, respectively. The corresponding expression for subordinate lines (for which both the levels are radiatively and collisionally broadened), was derived by Heinzel & Hubeny (1982). It is expressed as a linear combination of functions $R_{\mathrm{V}-A}(x, x')$ and $R_{\mathrm{II}-A}(x, x')$, with a branching ratio Λ now computed taking account of broadening of both the levels. It is written as

$$R(x, x') = \Lambda R_{\mathrm{V}-A}(x, x') + (1 - \Lambda) R_{\mathrm{III}-A}(x, x') \, . \tag{24}$$

It is clear that equation (22) is a special case of equation (24). A detailed study of collisional redistribution on resonance and subordinate lines is made by Hubeny & Heinzel (1984). The equations (22) and (24) represent good approximations to study the collisional effects on line formation. They are widely used in astrophysical literature. In recent years more exact formulations of the collisional redistribution functions have been developed.

We shall now discuss a redistribution matrix which correctly takes into account the effect of collisions. Domke & Hubeny (1988), and Streater et al. (1988) developed very general angle-dependent redistribution matrices, which represent the radiative and collisional redistribution of an arbitrarily polarized beam of light. We shall give below the expressions which help us compute angle-averaged version of the general Domke–Hubeny redistribution matrix which is employed in this paper. The general Domke–Hubeny (DH) redistribution matrix is written as

$$\begin{aligned} \boldsymbol{R}_{\mathrm{DH}}(x, \mu, x', \mu') = {} & W_2 \alpha [R^A_{\mathrm{II}}(x, \mu, x', \mu') \hat{\boldsymbol{P}}^A(\mu, \mu') + R^B_{\mathrm{II}}(x, \mu, x', \mu')) \hat{\boldsymbol{P}}^B(\mu, \mu') + R^C_{\mathrm{II}}(x, \mu, x', \mu') \hat{\boldsymbol{P}}^C(\mu, \mu')] \\ & + (1 - W_2) \alpha [R^A_{\mathrm{II}}(x, \mu, x', \mu') \hat{\boldsymbol{P}}^I(\mu, \mu')] + W_2 \beta^{(2)} [R^A_{\mathrm{III}}(x, \mu, x', \mu') \hat{\boldsymbol{P}}^A(\mu, \mu') + R^B_{\mathrm{III}}(x, \mu, x', \mu') \hat{\boldsymbol{P}}^B(\mu, \mu') + R^C_{\mathrm{III}}(x, \mu, x', \mu') \hat{\boldsymbol{P}}^C(\mu, \mu')] \\ & + (\beta^{(0)} - W_2 \beta^{(2)}) [R^A_{\mathrm{III}}(x, \mu, x', \mu') \hat{\boldsymbol{P}}^I(\mu, \mu')] \, , \end{aligned} \tag{25}$$

where the angular phase matrices are given by

$$\hat{\boldsymbol{P}}^A(\mu, \mu') = -\frac{3}{2} \begin{pmatrix} 0 & 1 \\ 1 & 0 \end{pmatrix} ; \quad \hat{\boldsymbol{P}}^B(\mu, \mu') = \begin{pmatrix} 1 & 1 \\ 1 & 1 \end{pmatrix} ; \quad \hat{\boldsymbol{P}}^C(\mu, \mu') = \frac{3}{2} \begin{bmatrix} 0 & (1 - \mu^2) \\ (1 - \mu'^2) & -(\mu^2 + \mu'^2) \end{bmatrix} ; \quad \text{and} \quad \hat{\boldsymbol{P}}^I(\mu, \mu') = \begin{pmatrix} 1 & 0 \\ 0 & 0 \end{pmatrix} . \tag{26}$$

The frequency redistribution functions in equation (25) are defined as

$$R^A_{\mathrm{II,III}}(x, \mu, x', \mu') = \frac{1}{2\pi} \int_0^{2\pi} R_{\mathrm{II,III}}(x, \mu, x', \mu', \Delta) 1 \, d\Delta \, , \tag{27a}$$

$$R^B_{\mathrm{II,III}}(x, \mu, x', \mu') = \frac{1}{2\pi} \int_0^{2\pi} R_{\mathrm{II,III}}(x, \mu, x', \mu', \Delta) \frac{3}{4} (1 + \cos^2 \Theta) d\Delta \, , \tag{27b}$$

$$R^C_{\mathrm{II,III}}(x, \mu, x', \mu') = \frac{1}{2\pi} \int_0^{2\pi} R_{\mathrm{II,III}}(x, \mu. x', \mu', \Delta) \sin^2 \Delta \, d\Delta \, . \tag{27c}$$

If we substitute $\boldsymbol{R}_{\mathrm{DH}}$ in equation (1) and employ Rees-Saliba prescription (eq. [2]) for angle and frequency decoupling, then these equations (27) become equivalent to equations (6). The DH redistribution function refers to the radiative and collisional (elastic and inelastic) redistribution process in resonance lines ($a_u \neq 0$ and $a_l = 0$). The thermalization parameter ϵ is related to the collisional parameters through the relation

$$\epsilon = \frac{\epsilon'}{1 + \epsilon'} \qquad \text{with} \qquad \epsilon' = \frac{\Gamma_I (1 - e^{-h\nu_0/kT_e})}{\Gamma_R} \, . \tag{28}$$

The branching ratios appearing in equation (25) for DH redistribution matrix are listed below:

$$\alpha = \frac{\Gamma_R}{\Gamma_R + \Gamma_I + Q_E}, \tag{29}$$

where α is the probability that reemission of radiation occurs before any type of collision. Scattering is thus coherent in the atomic frame,

$$\beta^{(0)} = \alpha \frac{Q_E}{\Gamma_R + \Gamma_I}, \tag{30}$$

where $\beta^{(0)}$ is the probability that reemission occurs after an elastic collision but before an inelastic quenching collision occurs. In this case, the correlations between frequencies of absorbed and emitted photons are destroyed by elastic collisions. Therefore scattering causes a complete redistribution in the atomic frame,

$$\beta^{(2)} = \alpha \frac{Q_E - D^{(2)}}{\Gamma_R + \Gamma_I + D^{(2)}}, \tag{31}$$

where $\beta^{(2)}$ is the probability that reemission occurs after the elastic collision that changes the phase of oscillating atomic dipole, but does not change the alignment. In this case, also, as with the case of $\beta^{(0)}$, scattering causes a complete redistribution of the atomic frame. The quantity $D^{(2)}$ is the rate of elastic collisions that destroy alignment.

The sum of composite branching ratios (the factors which multiply the terms inside the square brackets in eq. [25]), which decouple type II and type III redistribution functions of Hummer, in equation (25), is given by

$$W_2\,\alpha + (1 - W_2)\alpha + W_2\,\beta^{(2)} + [\beta^{(0)} - W_2\,\beta^{(2)}] = \alpha + \beta^{(0)} = \frac{\Gamma_R}{\Gamma_R + \Gamma_I} = (1 - h)\,; \qquad h = \frac{\Gamma_I}{\Gamma_R + \Gamma_I}, \tag{32}$$

It is traditional in astrophysical formalism of line formation theory to work always in terms of normalized redistribution functions. Equation (25) is not normalized to unity when integrated over the solid angles representing incoming and outgoing directions of the photons. The reason for this is that, the composite branching ratios α, $\beta^{(0)}$ and $\beta^{(2)}$ do not satisfy $\alpha + \beta^{(0)} = 1$, unless $h = 0$ (see eq. [32] above). Now, to be consistent with the equation (1), we have to renormalize these branching ratios as follows:

$$\frac{\alpha}{(1 - h)} = \bar{\alpha} = \frac{\Gamma_R + \Gamma_I}{\Gamma_R + \Gamma_I + Q_E}, \tag{33}$$

$$\frac{\beta^{(0)}}{(1 - h)} = \bar{\beta}^{(0)} = \frac{Q_E}{\Gamma_R + \Gamma_I + Q_E} = (1 - \bar{\alpha})\,, \tag{34}$$

$$\frac{\beta^{(2)}}{(1 - h)} = \bar{\beta}^{(2)} = \bar{\alpha}\,\frac{Q_E - D^{(2)}}{\Gamma_R + \Gamma_I + D^{(2)}}\,. \tag{35}$$

The new renormalized branching ratios $\bar{\alpha}$, $\bar{\beta}^{(0)}$, and $\bar{\beta}^{(2)}$ now satisfy the normalization condition

$$W_2\,\bar{\alpha} + (1 - W_2)\bar{\alpha} + W_2\,\bar{\beta}^{(2)} + (\bar{\beta}^{(0)} - W_2\,\bar{\beta}^{(2)}) = 1\,. \tag{36}$$

In order to use the DH redistribution matrix in the normalized form, in equation (1), we have to replace the original branching ratios α, $\beta^{(0)}$, and $\beta^{(2)}$ by the corresponding quantities $\bar{\alpha}$, $\bar{\beta}^{(0)}$, and $\bar{\beta}^{(2)}$, respectively. It is useful to note that the redistribution functions derived by quantum mechanical studies (for example the functions derived by Omont et al. 1972, and by Domke & Hubeny 1988) are unnormalized. They are defined, to start with, in such a way that they do not necessarily have to be normalized to unity. A detailed discussion of this important question of normalization of redistribution functions is presented in Hubeney & Cooper (1986). The author is grateful to the referee for clarifying the essentials of this question of normalization of redistribution functions. A given transition is characterized by the parameters Γ_R, Γ_I, Q_E, and W_2. They can be computed exactly using the quantum mechanical calculations (see Domke & Hubeny 1988). Since we are interested in the parameterized study of collisional effects, we use simple expressions which give rough estimates of these quantities. We have taken these formulae mainly from Faurobert-Scholl (1992), who have studied the Ca I and Sr I line formation problem in a realistic solar atmosphere.

Γ_R is the radiative de-excitation rate (or natural width) of the upper level u. The quantity Γ_I is the rate of inelastic quenching collisions of perturbing atoms with the radiating atom, which result in the destruction of alignment (see Domke & Hubeny 1988). Γ_I and Γ_R are related through equation (28). The quantity $Q_E (= \Gamma_C)$ is the rate of elastic collisions which result in collisional broadening of the upper level u. If, for example, the elastic collisional damping is due to collisions with neutral hydrogen atoms (as is true in most astrophysical plasmas), then we can employ

$$Q_E = \Gamma_C \cong \gamma_{\rm VW}\, N_{\rm H} (T_e/5000)^{0.3}\,, \tag{37}$$

where $\gamma_{\rm VW}$ is the Van der Waal's coefficient and $N_{\rm H}$ the number density of hydrogen atoms. A simple relation

$$D^{(2)} \simeq 0.758 (Q_E/2)\,, \tag{38}$$

given in Faurobert-Scholl (1992), is employed by us for computing the factor $D^{(2)}$. Now, the total damping parameter a that should

be employed when doing computations with DH redistribution functions, is given by (with $a_l = 0$ for resonance lines)

$$a = a_{ul} = (a_u + a_l) = \frac{\Gamma_R + \Gamma_C}{4\pi \Delta\nu_D} . \tag{39}$$

Finally we have

$$W_2 \equiv E_1 . \tag{40}$$

where W_2 is the probability that intrinsic "level depolarization" does not occur during scattering. Notice that W_2 can also be computed from expressions for E_1 given in Chandrasekhar (1960), or Ballagh & Cooper (1977). E_1 basically depends on the angular momentum quantum numbers j_l and j_u of the transition involved. Clearly, as seen from equation (4), maximum polarization occurs for transitions of the type ($j_u = 1 \rightarrow j_l = 0$), for which $E_1 = 1$.

It is useful to note that DH redistribution matrix can also be expressed in a simpler form, in some situations, for instance by making a deliberate choice of parameters:

$$W_2 = 1; \quad \text{and} \quad D^{(2)} = 0 . \tag{41}$$

With these choices, we get

$$\bar{\alpha} = \Lambda ; \quad \text{and} \quad \bar{\beta}^{(0)} = \bar{\beta}^{(2)} = (1 - \Lambda) . \tag{42}$$

As a result, the normalized version of equation (25) can be rewritten in the form

$$\boldsymbol{R}_{\rm DH}(x, \mu, x', \mu') = \Lambda[R^A_{\rm II}(x, \mu, x', \mu')\hat{\boldsymbol{P}}^A(\mu, \mu') + R^B_{\rm II}(x, \mu, x', \mu')\hat{\boldsymbol{P}}^B(\mu, \mu') + R^C_{\rm II}(x, \mu, x', \mu')\hat{\boldsymbol{P}}^C(\mu, \mu')] + (1 - \Lambda)$$
$$\times [R^A_{\rm III}(x, \mu, x', \mu')\hat{\boldsymbol{P}}^A(\mu, \mu') + R^B_{\rm III}(x, \mu, x', \mu')\hat{\boldsymbol{P}}^B(\mu, \mu') + R^C_{\rm III}(x, \mu, x', \mu')\hat{\boldsymbol{P}}^C(\mu, \mu')] , \tag{43}$$

which is nothing but collisional redistribution analogue of the collisionless redistribution matrix (see eq. [7]). This statement can be verified by substituting collisional redistribution function, $R(x, x')$ given by equation (22), in equation (7).

For the sake of discussion of different collisional effects, we can rewrite the DH redistribution matrix (eq. [25]) in the following form (dropping some of the arguments for clarity):

$$\boldsymbol{R}_{\rm DH} = C_1[R^A_{\rm II}\hat{\boldsymbol{P}}^A + R^B_{\rm II}\hat{\boldsymbol{P}}^B + R^C_{\rm II}\hat{\boldsymbol{P}}^C] + C_2[R^A_{\rm II}\hat{\boldsymbol{P}}^I] + C_3[R^A_{\rm III}\hat{\boldsymbol{P}}^A + R^B_{\rm III}\hat{\boldsymbol{P}}^B + R^C_{\rm III}\hat{\boldsymbol{P}}^C] + C_4[R^A_{\rm III}\hat{\boldsymbol{P}}^I] , \tag{44}$$

where the constants C_1, C_2, C_3, and C_4 are defined as

$$C_1 = W_2\bar{\alpha} ; \quad C_2 = (1 - W_2)\bar{\alpha} ; \quad C_3 = W_2\bar{\beta}^{(2)} ; \quad C_4 = (\bar{\beta}^{(0)} - W_2\bar{\beta}^{(2)}) .$$

Equation (44) can be written formally as

$$\boldsymbol{R}_{\rm DH} = C_1[R_{\rm II}(\text{anisotropic})] + C_2[R_{\rm II}(\text{isotropic})] + C_3[R_{\rm III}(\text{anisotropic})] + C_4[R_{\rm III}(\text{isotropic})] . \tag{45}$$

This equation can also be written in another conventional form as

$$\boldsymbol{R}_{\rm DH} \approx \Lambda_{\rm II}\langle R_{\rm II}\rangle_{\rm av} + \Lambda_{\rm III}\langle R_{\rm III}\rangle_{\rm av} , \tag{46}$$

where $\langle\cdots\rangle_{\rm av}$ is some kind of weighted average whose functional form is not of consequence for the present purpose. The branching ratios of equation (46) are then given by

$$\Lambda_{\rm II} = C_1 + C_2 = \bar{\alpha} , \tag{47a}$$

which is the coherence fraction. The noncoherence fraction is

$$\Lambda_{\rm III} = C_3 + C_4 = (1 - \Lambda_{\rm II}) = \bar{\beta}^{(0)} . \tag{47b}$$

The interpretational significance, of the renormalized branching ratios $\bar{\alpha}$, $\bar{\beta}^{(0)}$, and $\bar{\beta}^{(2)}$, is not straightforward and simple, in the same way as normalized redistribution functions (see Hubeny & Cooper 1986). However, we can write $\bar{\alpha}$, $\bar{\beta}^{(0)}$, and $\bar{\beta}^{(2)}$ as

$$\bar{\alpha} = \alpha + \delta , \tag{48}$$

$$\bar{\beta}^{(0)} = (1 - \alpha) - \delta , \tag{49}$$

$$\bar{\beta}^{(2)} = \beta^{(2)} + \delta\frac{Q_E - D^{(2)}}{\Gamma_R + \Gamma_I + D^{(2)}} , \tag{50}$$

where

$$\delta = \frac{\Gamma_I}{\Gamma_R + \Gamma_I + Q_E} . \tag{51}$$

The factor $\delta \rightarrow 0$ when $\Gamma_I \ll (\Gamma_R, \Gamma_C)$, a condition which is satisfied for all the models presented in this paper, except for models 3–6 in Figure 3 (see Table 1 also). Hence C_1, C_2, C_3, and C_4 can be used to understand the results of our computations. The physical significance of all the terms of DH redistribution matrix are explained in Domke & Hubeny (1988; the paragraph that follows their equations [49]–[52]).

TABLE 1

EFFECT OF VARIATION OF INELASTIC COLLISIONAL RATE Γ_I [a]

Model	ϵ	Γ_I (Hz)	C_1	C_2	C_3	C_4	Λ_{II}	x_{FT}	τ_{FT} ($\times 10^3$)	x_{PD}	τ_{PD}	x_{CS}	T_{eff}
1.....	0.0000	0	0.499	0.055	0.191	0.255	0.55	3.2	3.2	3.20	3.2×10^3	5.64	0
2.....	0.0001	2×10^4	0.499	0.055	0.191	0.255	0.55	3.2	3.2	3.20	3.2×10^3	5.64	1.0×10^2
3.....	0.3333	1×10^8	0.586	0.065	0.162	0.187	0.65	1.7	0.52	0.31	3.0	5.64	3.3×10^5
4.....	0.5000	2×10^8	0.642	0.071	0.139	0.148	0.71	1.4	0.28	0.27	2.0	5.64	5.0×10^5
5.....	0.6667	4×10^8	0.710	0.079	0.107	0.104	0.79	1.2	0.18	0.25	1.5	5.64	6.7×10^5
6.....	0.9999	2×10^{12}	~0.9	~0.1	5×10^{-5}	4×10^{-5}	~1	~1	0.10	0.22	~1	5.64	1.0×10^6

[a] $\Gamma_R = 2 \times 10^8$ Hz, $\Gamma_C = 1.6 \times 10^8$ Hz, $\Delta\nu_D = 2.9 \times 10^9$ Hz, $D^{(2)} = 0.61 \times 10^8$ Hz, $W_2 = 0.9$, $T_{eff} = \epsilon T^L$, $x_{FT} = \min [x_\epsilon, x_{\beta^C}]$ and $\tau_{FT} = \min [\tau_\epsilon, \tau_{\beta^C}] = \min [\tau_\epsilon(x_\epsilon), \tau_{\beta^C}(x_{\beta^C})]$, $x_{PD} = \min [x_{th}, x_{\beta^C}]$ and $\tau_{PD} = \min [\tau_{th}, \tau_{\beta^C}] = \min [\tau_{th}(x_{th}), \tau_{\beta^C}(x_{\beta^C})]$.

For a study of the effect of collisions on subordinate lines, we follow an approach suggested by Hubeny & Heinzel (1984), according to which equation (24) is substituted in equation (7), to obtain the corresponding redistribution matrix. For simplicity, we have not explicitly computed Λ, but selected certain values in the range $(0 \leq \Lambda \leq 1)$ for a parametric study involving equations (22) and (24). Note that explicit relations are given in Hubeny & Heinzel (1984) for computing the branching ratio Λ in terms of various radiative and collisional rates, in a general picture of three-level atom. In passing we note that collisional redistribution model employed by Saliba (1985) is a special case of DH model when $\bar{\beta}^{(2)} = 0$, that is, when $Q_E = D^{(2)}$ in equation (35). In other words his model represents an extreme case where all the elastic collisions are completely depolarizing.

3. RESULTS AND DISCUSSION

In this section we have several subsections, each one of which addresses a specific aspect of the problem. Each subsection is self-contained in this way. However, the general role of collisional redistribution is highlighted so that this topic is appreciated in the context of variation of each set of model parameters. Obviously the cases studied are theoretically oriented and sometimes may be far from realistic situations. The main idea, therefore, is to understand general theoretical features of polarization profile when collisional effects are dominant. For the sake of uniformity in convention we always refer to intensity, for example, as $I(x, \mu, r)$ instead of $U(x, \mu, r)$. The percentage of linear polarization is referred to as $p(x, \mu, r) = [Q(x, \mu, r)/I(x, \mu, r)] \times 100$. All the results correspond to lines formed in a spherically symmetric shell atmosphere whose outer radius is 3 times the inner radius ($R = 3$). The shell is bounded on the inner side by an isotropically emitting photosphere. The central core of the spherical shell is thus an opaque emitting sphere. This picture resembles the conventional extended stellar atmospheres of stars. The spherical shell is assumed to be a gray and isothermal $[B(r) = 1]$ medium. All the opacities are taken to vary according to an inverse square law ($\chi^{L,C,e}(r) = \chi r^{-2}$), where the constant $\chi = RT^L/(R-1)$. Hence the opacity ratios β^C and β^e remain spatially constant in the atmosphere. All the important line formation parameters, namely, broadening parameters (e.g. $a, \Delta\nu_D, \Gamma_R, \Gamma_C$, etc.), branching ratios, coupling constants, atomic and electron number densities (see § 2), are also assumed to have constant values in the spherical shell atmosphere. Results are shown on a smaller frequency bandwidth ($0 < x < 10$) except when electron scattering is considered. We have employed a nonuniform frequency grid with 27–35 frequency points in the half space ($0 < x < x_{max}$) depending on the model. A logarithmically spaced optical depth grid with 45 or 61 points, depending on the situation, is employed. A three-point Gaussian quadrature in the range $\mu \in (0, 1)$ is used in the angle integration of the transfer equation. The angular resolution of three Gaussian points per quadrant is sufficient for the kind of SS models considered in this paper. The models are characterized by small values of $R(= 3)$, large values of T^L and opacity power-law index $n = 2$. This selection of global parameters, supplemented by the Schuster's boundary condition, and the presence of strong continuous absorption make the effects of angular peaking of the radiation field in SS models negligible for most part of the line (see Mihalas et al. 1975). Hence there is no demand for a larger number of angle points here. However, when we consider small values of T^L, larger values of R, and $n \geq 2$, we must take a larger number of angle points, since peaking of radiation in outer layers leads to serious problems.

All the frequency and angle integrals that occur in the elementary redistribution functions are evaluated accurately to ensure smooth and accurate representation of redistribution integral in equation (1). These functions, as well as the emergent specific intensities and polarizations obtained after using them in radiative transfer computations, are checked by comparing the results with the published models (cf. Heinzel & Hubeny 1982, 1983; Hubeny & Heinzel 1984; Faurobert-Scholl 1987, 1988, etc.). Also, the electron scattering is neglected ($\beta^e = 0$) for all the figures except Figure 9. All of our models (excepting few cases) represent an effectively thick line emission ($\epsilon T^L = 10^2 \gg 1$). Further, the continuum is also effectively thick ($T^C = \beta^C T^L = 10^2 \gg 1$) resulting in the presence of strong unpolarized continuum radiation throughout the atmosphere. The continuum radiation, when escaping directly in the wings, can easily drive the wing polarization to zero. However, when it it repolarized upon scattering on atoms (and electrons) in the atmosphere, it can lead to a complex frequency dependence in line wing polarization. Unlike monochromatic line optical depth $[\tau_x^L = \phi(x)T^L]$, the continuum optical depth is frequency independent. For the sake of convenience, we have used the symbol τ everywhere instead of τ^L to represent the average optical depth variable.

We discuss our results mainly through emergent intensity and polarization profiles $I(x, \mu_1 = 0.11, \tau = 0)$ and $p(x, \mu_1 = 0.11, \tau = 0)$. It is also useful to present some macroscopic quantity, that characterizes a given model, namely, the optical depth dependence of source functions $S_I(\tau)$ which is an angle and frequency-integrated source function for scalar intensity. In the third panel of each figure we show the depth dependence of $S_I(\tau)$. In the fourth panel we have plotted a quantity $Z(\tau) = S_Q(\tau)/S_I(\tau)$ which is a measure of the total anisotropy of the source function in the atmosphere (see Rees 1978). It is well known that the angle-dependent emergent intensities $I(x, \mu, \tau)$ and $Q(x, \mu, \tau)$ can be related to the respective source functions $S_{I,Q}[x, \mu, \tau = \mu/\phi(x)]$ according to the

Eddington-Barbier relation. This relation can be used to interpret the qualitative aspects of the emergent intensity and polarization (i.e., limb darkening/brightening, sign changes of polarization profile, etc.). But we have preferred to plot the integrated quantities $S_I(\tau)$ and $Z(\tau)$, instead of $S_{I,Q}(x, \mu_1 = 0.11, \tau)$ at selected frequencies, because it is instructive to know the march of anisotropy inside the atmosphere in general, since it is the optical depth gradient of the source function $S_I(\tau)$ (in other words the gradient of temperature, etc.), that affect strongly the degree of emergent polarization than other factors. The source function $S_Q(\tau)$ represents the source of Q-component of the intensity generated locally as well as inscattered nonlocally from other depth points. Thus the ratio $Z(\tau)$ represents the rate of generation of local anisotropy or linear polarization.

It is important to note that the scaling laws used in this paper, to interpret the results, are borrowed from the plane parallel (PP) case. In principle we must use the corresponding expressions derived for a spherically symmetric (SS) case. The situations under which PP scaling laws can also be used, as a first approximation, to interpret the SS results are that (1) single flight escape probability factors of PP and SS cases should be of same order of magnitude, (2) the ratio of the probablity of outward scattering to the probability of inward scattering-bias factor in SS should approach unity (it is exactly equal to unity in PP case), (3) the monochromatic spherical dilution factor should be of order unity across the bandwidth of the line, and (4) the mean number of scatterings, the mean escape probability, and thermalization length, etc., should be of the same order of magnitude as the corresponding PP case. Simple expressions are derived in Kunasz & Hummer (1974) for checking these four criteria mentioned above. All the four criteria are satisfied for the models presented in this paper. However, care should be taken, when using the PP scaling laws or escape probability arguments, in the SS case. The validity criteria mentioned above strongly depend on R, T^L, n, m, and ϵ, where n and m are the power-law indices for radial dependence of opacity and Planck function. The "bias" in particular should not differ much from unity. In a PP atmosphere scattering according to the CRD mechanism, a photon created near the line center does not typically move far from its point of creation while undergoing frequency redistribution and finally escapes from the medium in "single longest flight." This provides the theoretical basis for CRD escape probability methods in PP slabs. In SS systems, on the other hand, the bias leads to steady outward drift of photons as they are scattered, undermining the relevance of the single longest flight. This makes the escape probability methods using this concept less reliable for SS atmospheres with large bias. In the absence of a well-developed theory of PRD frequency thermalization in spherical geometry, we can perhaps use the probabilistic expressions derived for PP slabs, as a first approximation, but only in cases where the four validity criteria mentioned above are satisfied. Seen in this perspective, the probabilistic quantities given in Tables 1–7 are intended as a guide, rather than a means, of interpreting the results computed by explicit solution of the SS transfer problems.

3.1. *A Comparison of Lines Formed under Elementary Redistribution Mechanisms*

In this section we study some of the redistribution mechanisms mentioned in § 2.2. The results are shown in Figure 1. The profiles formed with R_{II-A} redistribution represented by long dashed lines merge with the pure coherent scattering (CS) profiles (dotted lines) in the far wings of the line ($x > 6$). This is due to the wing coherence exhibited by R_{II-A} redistribution function in general. The intensity profile of CS is deepest of all the functions considered, and CS also corresponds to the largest degree of polarization (p) in both the line core ($x < 3$) and line wings ($x > 3$). The frequency coherence during scattering is not directly related to the larger degree of polarization. Indeed it is mainly the source function gradient, along with the frequency coherence that can directly lead to a larger degree of linear polarization in the line. However, the frequency coherence can inhibit more effectively the global mixing of positively and negatively polarized photons, compared to other PRD mechanisms. Due to this reason, CS represents, at least in the line core, an upper limit on the degree of linear polarization. In a narrow frequency range of $x < 0.6$, however, R_{III-A} has a slightly larger emission probability than even CRD. Due to this and larger correlations between incoming and outgoing photons, caused by Doppler motion of atoms, the derivations of R_{III-A} polarization profiles from CRD are quite large in the line core. Since R_{II-A} has a degree of coherence next only to CS, the absolute values of polarization due to this mechanism is always larger than polarization due to other mechanisms except CS in the entire frequency bandwidth. However, interesting situation of CRD polarization being larger than the R_{II-A} polarization in the range $x < 0.3$ occurs when a negligible amount of continuum opacity is present in the atmosphere (see Faurobert-Scholl 1988, Fig. 1; Nagendra 1988, Fig. 13). The presence of a strong continuum opacity as we do have now contributes positively polarized photons to emergent polarization. The formation of subordinate lines with R_{V-A} redistribution function is discussed in detail by Hubeny & Heinzel (1984). The results for semi-infinite slabs and $(a_u/a_l) = 10$ in their paper are useful in understanding the results of our computations [$T^L = 10^6$ and $(a_u/a_l) = 9$ in our models]. The intensity and polarization profiles of R_{V-A} do not differ greatly from corresponding R_{II-A} profiles. The emergent polarization profiles calculated with the function R_{V-A} lie between those of R_{II-A} and CRD, in the same way as the intensity profile. This behavior confirms the conclusions of Hubeny & Heinzel (1984). However, the deparatures of R_{V-A} from CRD decreases gradually as $a_u \to a_l$. It is well known that the function R_{V-A} is characterized by an additional probability of a wing photon subsequent to an absorption, being reemitted in the vicinity of line center apart from a probability of being reemitted almost coherently in the wing itself, purely due to lower state broadening. The ratio of the probability of coherent reemission, to the reemission probability near line center is directly proportional to (a_u/a_l). This characteristic of resonance scattering in subordinate lines is also responsible for the very close similarity of R_{II-A} and R_{V-A} profiles in Figure 1, since clearly, R_{II-A} is a special case of R_{V-A} in the limit $(a_u/a_l) \to \infty$.

Now we look into the variation of source functions $S_I(\tau)$ and the polarization rate $Z(\tau)$ in Figure 1 as a function of optical depth $\tau(r)$ in the spherical shell. These two quantities together define the overall anisotropy existing inside the atmosphere of a given model. The sign of the anisotropy rate as a function of τ and the depth dependence are mapped into frequency dependence of the emergent polarization profile. This mapping function, however, neither is linear nor has a simple analytic form for general PRD transfer problems. The anisotropy rate for R_{II-A} is highest in most parts of the outer layers ($T < 100$), essentially where the line core is formed. However, in the region of the atmosphere where the near line wings are formed ($100 < \tau < 3 \times 10^4$), it is CS mechanism that corresponds to the largest rate of anisotropy. The anisotropy rate of the redistribution functions CS, R_{II-A} and R_{V-A} reach maxima somewhere in the range $10^3 < \tau < 3 \times 10^3$. On the other hand, for CRD the anisotropy rate is almost insignificant for

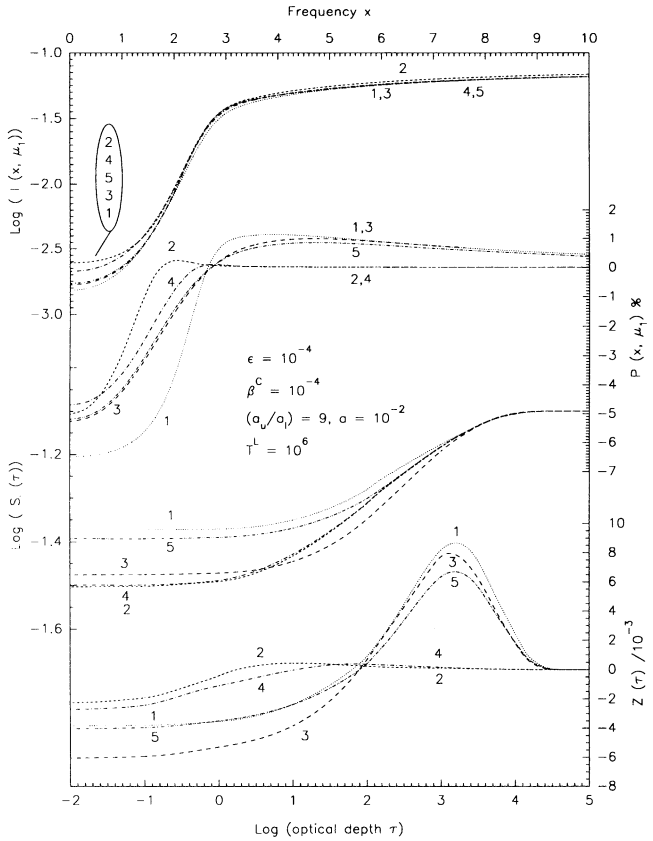

FIG. 1.—Line polarization for different redistribution mechanisms. Emergent intensity I and polarization p in the direction $\mu_1 = 0.11$ are shown in the first two panels. Abscissa for these two upper panels is the frequency x measured from line center in the units of a constant Doppler width. The model parameters are described in § 3. Some of the global parameters (ϵ, β^C, a, T^L, β^e) are shown inside the figure for easy reference. The electron scattering is neglected ($\beta^e = 0$). The lower two panels refer to the optical depth dependence of the intensity source function $S_I(\tau)$ and the polarization rate $Z(\tau)$ defined in the text. The abscissa for these two panels is logarithm of average optical depth variable τ. The numbers shown near the curves identify the models. Models (1)–(5) correspond respectively to the profiles computed using CS, CRD, R_{II}, R_{III}, and R_V redistribution functions. See § 3.1 for further details.

depths beyond $\tau = 10$, and for R_{III-A} beyond $\tau = 100$. For these noncoherent redistribution functions, it appears as though a thin polarizing layer of spherical shell surrounds a thick photospheric layer filled with unpolarized diffuse radiation field, when looked through the monochromatic optical depth scale $\tau(x)$, or even the average optical depth scale. Wing coherence, on the other hand, seems to be generally responsible for the peaking of anisotropy rate $Z(\tau)$ deep in the atmosphere for other redistribution mechanisms (see curves 1, 3, and 5).

The models presented in this paper are moderately optically thick $(aT^L)^{1/3} = 21.5$, as well as effectively thick $\epsilon T^L = 10^2$. Even the continuum is optically thick ($\beta^C T^L = 10^2$). Thus, it is necessary to indicate which of the parameters, namely, ϵ (acting through inelastic collisional de-excitation of atoms), or β^C (acting through continuum absorption/emission by atoms) controls transfer in the coherent line wings; in other words, to specify which parameter dominates the frequency thermalization of the source functions. Frequency thermalization (FT) refers to the frequency diffusion process leading to the arrival of PRD line wing photons at the line core, where subsequent line scatterings can well be described by CRD, before escaping from the medium. FT is very effective when line optical depths are large. To decide which of the two processes mentioned above is stronger, we compare $\tau_{\beta C}(x_{\beta C})$ and $\tau_\epsilon(x_\epsilon)$ the characteristic depths at characteristic frequencies $x_{\beta C}$ and x_ϵ, respectively (Hubeny 1985a). The characteristic depth of frequency thermalization of the source functions is given by $\tau_{FT} = \min [\tau_\epsilon(x_\epsilon), \tau_{\beta C}(x_{\beta C})]$, where $\tau_{\beta C}(x_{\beta C}) \approx a^{-1/4}(\beta^C)^{-3/4} = 3.2 \times 10^3$ and $\tau_\epsilon(x_\epsilon) \approx a^{-1}\epsilon^{-3/2} = 10^8$, that is, $\tau_{FT} = 3.2 \times 10^3$. From Figure 1 it can be seen that at this optical depth, the distinction between source functions $S_I(\tau)$ corresponding to different redistribution mechanisms is negligible and only the anisotropy rate $Z(\tau)$ is useful in the study of depth variation of source functions. The characteristic frequency for frequency thermalization of intensity given by $x_{FT} = \min [x_\epsilon, x_{\beta C}] \approx \min [\epsilon^{-1/2}, a^{1/4}(\beta^C)^{-1/4}] = \min [100, 3.2] = 3.2$. Thus, clearly, the continuum absorption (β^C) controls the frequency thermalization of the line wing photons. Similarly, the characteristic depth of photon destruction is given by $\tau_{PD} = \min [\tau_{th}(x_{th}), \tau_{\beta C}(x_{\beta C})] \approx \min [\epsilon^{-1}, a^{-1/4}(\beta^C)^{-3/4}] = \min [10^4, 3.2 \times 10^3] = 3.2 \times 10^3$, and the characteristic frequency of photon destruction is given by $x_{PD} = \min [x_{th}, x_{\beta C}) \approx (a^{1/3}\epsilon^{-1/3}, a^{1/4}(\beta^C)^{-1/4}] = \min [4.6, 3.2] = 3.2$. In these expressions, x_{th} and $\tau_{th}(x_{th})$ refer to the loss of line photons to the thermal pool. Here again we see that the continuum absorption (β^C) controls the photon destruction process. Hence the transfer in the line wings in our saturated models ($T^L \gg \tau_{FT}$; $T^L \gg \tau_{PD}$) is controlled largely by the continuum radiation field.

Note also that the frequency point beyond which the overlapping continuum radiation dominates the total source function, and where the residual PRD line contribution represened by R_{II-A} can be treated as just coherent scattering, is given by $x_{CS} \approx$

$(\pi\beta^C/a)^{-1/2} = 5.6$, a behavior that can be clearly seen in the polarization profiles. It is known that the physical properties of a medium can affect the emergent intensity and polarization at frequency x, mainly in the optical depth interval $[\phi(x)]^{-1} < \tau < \tau_{FT}(x)$, where $[\phi(x)]^{-1}$ is the mean optical depth T^L that corresponds to the monochromatic optical depth $\tau(x)$ being equal to unity at frequency x. The quantity $\tau_{FT}(x)$ is given by $\tau_{FT}(x) \approx \pi x^3/(4a)$. Thus, for example, the polarization at frequency point $x = 10$ is mainly due to contributions from source functions in the depth range $(4.5 < \log \tau < 4.9)$. From the curves of anisotropy rate $Z(\tau)$ it is clear that the polarization gradually tends to zero in our models for frequencies $x > 10$. It is useful to note that for frequency points beyond $x = 10$, the mean free path of the photon between two consecutive scatterings is given by $l(x) \simeq [\phi(x)]^{-1} \simeq \pi x^2/a = 3.14 \times 10^4$. Due to this, the photons of frequency $x > 10$ suffer very small number of scatterings when they are produced in layers $\tau < l(x)$, and the dominant contribution from the deeper layers $\tau > l(x)$, which in turn have negligible anisotropy, naturally leads to negligible polarization in the far wings. Finally we make a general remark that the polarization and intensity profiles provide together a sensitive check on the usefulness of scaling laws and asymptotic analysis, than scalar intensity profiles alone. The condition for the importance of PRD effects in line scattering, as compared to continuous absorption effects, given by $\beta^C \ll a/\pi^2$ is satisfied by our models $(10^{-4} \ll 10^{-3})$. Thus all these models are scattering dominated. The essential features of redistribution and thermalization via multiple scattering are basically unaffected by the geometry of the medium. The important differences between polarized line formation in a SS media and a PP media is discussed in Nagendra (1988). It is helpful to refer to some of the models in that paper, where continuum absorption plays a much stronger role in the wing polarization behavior, than the models presented here.

3.2. *A Simple Treatment of the Effect of Collisions on Polarization in Resonance and Subordinate Lines*

The transfer problem in planar media, with noncoherent scattering in subordinate lines, including collisional effects, is well explored in Hubeny & Heinzel (1984). A study of subordinate lines basically involves at least a three-level atom model. The branching ratio Λ is thus in general a function of radiative and collisional rates of all the three levels. In this picture, the transitions to other states from the lower level leads to a broadening of the original subordinate line we are interested in. However, we have followed the approximate two-level approach suggested in Hubeny & Heinzel (1984). In Figure 2 we show qualitatively the effect of collisions on resonance and subordinate lines. The effect of collisions is incorporated simply through a branching ratio Λ between R_{II-A} (or R_{V-A}) and R_{III-A}, as suggested in equation (22) or (eq. [24]). A factor Λ that combines R_{II-A} and R_{III-A} in a laboratory frame is called coherence fraction. An exact treatment of collisional redistribution in subordinate lines is developed in Heinzel &

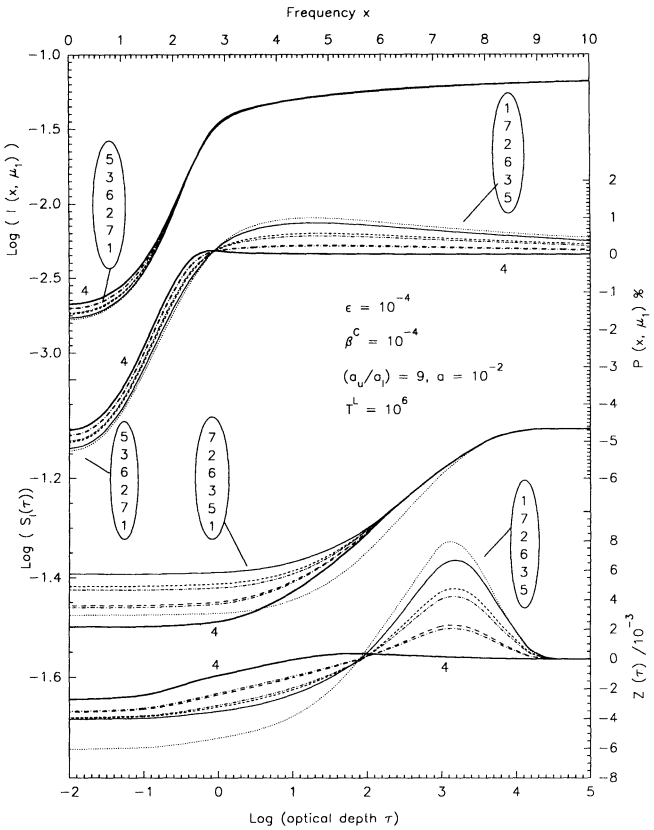

FIG. 2.—Effect of collisions on line polarization. The figure shows the same quantities as in Fig. 1. The collisional effects are included through a simple parameterized model, with branching ratio Λ between (R_{II}, R_{III}) or (R_V, R_{III}), being treated as an independent model parameter. Models (1)–(3) correspond respectively to the profiles computed for $\Lambda = 1, (\frac{2}{3}), (\frac{1}{3})$ between (R_{II}, R_{III}). Models (5)–(7) correspond, respectively, to the profiles computed for $\Lambda = (\frac{1}{3}), (\frac{2}{3}), 1$ between (R_V, R_{III}), respectively. Model 4 corresponds to the profiles computed for $\Lambda = 0$, which represents the pure R_{III} case. Results for model 4 are shown by thick solid lines. See § 3.2 for details.

Hubeny (1982) which is applicable even for resonance lines, since the latter is a special case of the former. The physical justifications and limitations for using a simple form as in equation (24) are given by Hubeny & Heinzel (1984). The difference between R_{II-A} polarization profile (dotted curves) and R_{V-A} profile (thin solid curve) is the same as that shown in Figure 1. Similarly the pair of curves corresponding to $R_{II+III}(\Lambda = \frac{2}{3})$ and $R_{V+III}(\Lambda = \frac{2}{3})$ differ by only a small amount, in fact lesser than the difference between pure R_{II-A} and R_{V-A} profiles. Similarly, the pair of curves $R_{II+III}(\Lambda = \frac{1}{3})$ and $R_{V+III}(\Lambda = \frac{1}{3})$ differ much less than the corresponding pair of curves for $\Lambda = \frac{2}{3}$. Finally the pure R_{III-A} case representing $\Lambda = 0$ (see curve 4) gives an upper limit of the extent to which the collisional redistribution (coupling with R_{III-A}) can affect the emergent line profiles in our models. It is clear that there are parameters (such as temperature) that vary in a stellar atmosphere, which can cause far more stronger changes in the line intensity and polarization profiles, than the atomic collisional effects alone. Nevertheless when a careful modeling of a line profile is necessary, it is better to take into account collisional effects, at very little extra computing effort, than being neglected. The $S_I(\tau)$ source functions of all the cases merge around $\tau = 10^2$, the depth at which the anisotropy rate also changes over sign from negative to positive.

Although it is known that the single flight escape probability concepts are not as useful for PRD as they are for CRD, they may be employed for reasonable estimates of the behavior of detailed radiative transfer computations. In the case of R_{II-A}, the majority of escaping photons get scattered to wing frequencies at fairly large optical depths itself, and then scatter nearly coherently many times while spatially diffusing out of the atmosphere. Since these so-called coherent scattering "excursions" begin deep inside the atmosphere for this particular case, the $S_I(\tau)$ source function of R_{II-A} case starts falling in magnitude compared to other PRD mechanisms including CS (see Fig. 1). In a series of papers Gayley (1992a, b, c) has developed the escape probability arguments for the PRD problem including collisional redistribution, generalizing the partial coherent scattering (PCS) approximation for PRD line transfer (see Hubeny 1985a). For our purposes, we just use a quantity called "single excursion frequency" $x_{SE}(\tau)$ defined in Gayley (1992a). It is the critical frequency for photon escape from a depth point τ. Most of the scatterings in the lifetime of a photon occur for frequencies $x < x_{SE}(\tau)$. When the photon is redistributed past the $x_{SE}(\tau)$, it escapes without further "redistributions." Adams (1972) showed that in the case of R_{II-A}, the overall PRD wing transfer can be described in terms of a "sequence" of nearly coherent scatterings "terminated" utlimately by a highly noncoherent event (which causes redistribution back to the line core). The sequence of coherent events at a stretch were shown to be equivalent to an effective "single longest excursion" between redistributions. The number of coherent events in a sequence [$\simeq 1/\Lambda_{RD}(x) \simeq 1/\Lambda_{DD}(x)$; for the special case of R_{II-A} it is $\approx x^2$] is not really great for near wing frequencies ($x < 10$) as compared to the mean number of scatterings ($\bar{N} \approx 3\tau/2$) required to traverse a mean optical depth τ. The quantity $\Lambda_{RD}(x)$ is the "redistribution" probability per scattering of a wing photon (in contrast to the destruction probability per scattering ϵ). Still, a coherent sequence can physically displace a photon by $1/[3\Lambda_{RD}(x)]^{1/2}$ (with a replacement RD $\rightarrow$ DD in case of R_{II-A}) mean free paths on the average. Thus $x_{SE}(\tau)$ is a critical frequency point for a given optical depth τ, which represents the last of a number of "coherent sequences" interspersed with (a smaller number of) "redistribution" events, for a photon, scattered to a frequency domain $x > x_{SE}(\tau)$, finally escapes from the medium without further redistribution. This general picture due to Adams (1972), devised originally for R_{II-A}, was shown by Gayley (1992a) to be applicable approximately to all types of PRD redistribution functions as long as wing scattering is largely coherent, and redistribution mechanism concerned can produce large frequency shifts in a single act of scattering. Starting from this hypothesis and by identifying the equivalence of single longest "flight" of the CRD escape probability theory, and the "single longest excursion" between redistributions in the PRD analog, Gayley (1992a) has derived the scaling laws for a wide range of redistribution mechanisms, namely, Doppler diffusion (DD, due to random motion of atoms), elastic scattering (ES, due to perturbation by charged particles–Stark effects; and perturbation by neutrals–Van der Waals broadening), inelastic scattering (IS, due to line interlocking in a multilevel atom model), etc. Using the conceptual advances made in representing the general PRD source function by the PCS approximation (Hubeny 1985a), new escape probability methods are developed in Gayley (1992b, c). Using the concept of PCS it is possible to derive appoximate PRD scaling laws for PRD redistribution functions, and their combinations thereof, in general (see Hubeny 1985a; Gayley 1992a, b, c). The $x_{SE}(\tau)$ at the mean optical depth τ is related to the general PRD redistribution probability $\Lambda[x_{SE}(\tau)]$ through the equation

$$\tau\phi[x_{SE}(\tau)] = \frac{1}{\sqrt{3\Lambda[x_{SE}(\tau)]}} . \tag{52}$$

For the special case of R_{II-A} where redistribution is purely due to the Doppler diffusion, the thermalization depth Σ_{DD} is given by $\Sigma_{DD} \simeq (1/\epsilon) = 10^4$ and the cutoff frequency at thermalization depth is given by $x_{SE}(\Sigma_{DD}) \simeq (a/\epsilon)^{1/3} = 4.6$. It can be noted that the so-called core/wing break point, or depth-dependent division frequency of Hubeny (1985a) corresponding to $\tau = \Sigma_{DD}$ is given approximately by $(a\Sigma_{DD})^{1/3} = 4.6$. Thus it appears that the frequency point where the polarization reaches positive maxima can be a reasonable indicator of the critical frequency point for R_{II-A} wing thermalization and the division frequency at R_{II-A} wing thermalization depth as long as a and ϵ remain nearly constant in the atmosphere. The strong coupling of frequency diffusion (roughly -1 Doppler width per scattering directed from wings to the core) and spatial diffusion, in the diffusion equation for R_{II-A} source function (see Frisch 1980), is specific to R_{II-A}. The inverse square variation of line and continuum opacity in SS case thus generally affects most strongly the R_{II-A} function compared to other functions.

3.3. *An Exact Treatment of the Effect of Collisions on a Resonance Line*

In this section we discuss the effect of collisions on resonance lines using the generalized redistribution matrix of Domke–Hubeny (1988) which we denote as $R_{DH-A}(x, x')$. Faurobert-Scholl (1992, 1993) has modeled the polarization observations of solar resonance lines using the DH redistribution matrix in a multilevel transfer problem solved in a realistic solar atmospheric model. Although ours is a parameterized study, the nature of parameterization is new, and we show the effect of variation of individual collision broadening mechanisms more clearly when the rest of the broadening parameters are held fixed. In these subsections (3.3.1–3.3.6)

the following constant model parameters are employed: $R = 3$; $T^L = 10^6$; $\beta^C = 10^{-4}$; $\beta^e = 0$; $B(r) = 1$; $T_e = 5000$ K; $\lambda = 5000$ Å; $\chi^{C,L}(r) = \chi r^{-2}$; $\boldsymbol{R} = \boldsymbol{R}_{\mathrm{DH}-A}$. The rest of the quantities required in two-level atom models are either fixed at the values shown below or parameterized as the case may be. These parameters are the following: $\epsilon = 10^{-4}$, $a = 10^{-2}$; $W_2 = 0.9$; mass of the radiating atom $M^a = 40$ amu; $\Delta\nu_{\mathrm{D}} = (\nu_0/c)(2kT_e/M^a)^{1/2} = 0.29 \times 10^{10}$ Hz (or parameterized by changing only M^a); $\Gamma_R = 2 \times 10^8$ Hz; $\Gamma_C = (4\pi a\,\Delta\nu_{\mathrm{D}} - \Gamma_R)$ Hz; $D^{(2)} = 0.379\Gamma_C$ Hz; $\Gamma_I = 2 \times 10^4$ Hz. The purpose of presenting a series of models in § 3.3 is to understand the way in which a selected "individual parameter" would affect a general collisional redistribution, when that parameter happens to be the most crucial one, oblivious of other parameters. It is clear that in reality, all the collisional parameters are multilaterally dependent on a host of other parameters. The dependence could be nonlinear in general depending on the state parameters of the plasma. In a realistic situation, the total collisional effect can thus be understood to be some kind of weighted average of the effects shown in §§ 3.3.1–3.3.6.

The thermalization scales x_{FT}, and τ_{FT} used in this paper are basically derived to describe the random walk of wing [where $\phi(x) \simeq a/\pi x^2$] photons. Further, except for models 3–6 in Table 1, all the models satisfy $x_{\mathrm{PD}} = x_{\mathrm{FT}}$, and $\tau_{\mathrm{PD}} = \tau_{\mathrm{FT}}$. Now, the four models 3–6 in Table 1, for which the characteristic frequencies x_{FT} are well within the line core, the global behavior of diffuse radiation field and source functions (thermalization information), are reflected in the usual thermalization scales x_{th} and $\tau_{\mathrm{th}}(x_{\mathrm{th}})$ derived assuming the creation and destruction of line photons during redistribution. As such, x_{FT} and τ_{FT} are not relevant for these four models. Indeed, even for the rest of the models in this paper, x_{FT} and τ_{FT} are only approximately valid, since x_{FT} values are sometimes quite small (~ 3). We hope that the statements above put our interpretation of numerical results, based on the PRD scaling laws, into the correct perspective.

3.3.1. *Effect of Variation of Inelastic Collisional Rate* (Γ_I)

The rate of inelastic quenching collisions Γ_I, which also destroy the alignment of the atom in the upper level, is directly related to the important parameter ϵ, the probability that a photon is destroyed by collisional de-excitation. So we have parameterized the variation of Γ_I through the equation

$$\Gamma_I(\epsilon) = \frac{\epsilon'\Gamma_R}{1 - e^{-(h\nu_0/kT_e)}}; \qquad \epsilon' = \frac{\epsilon}{1-\epsilon}, \tag{53}$$

where we have selected a series of values for ϵ, leading to the set of six curves shown in Figure 3. The characteristic parameters of

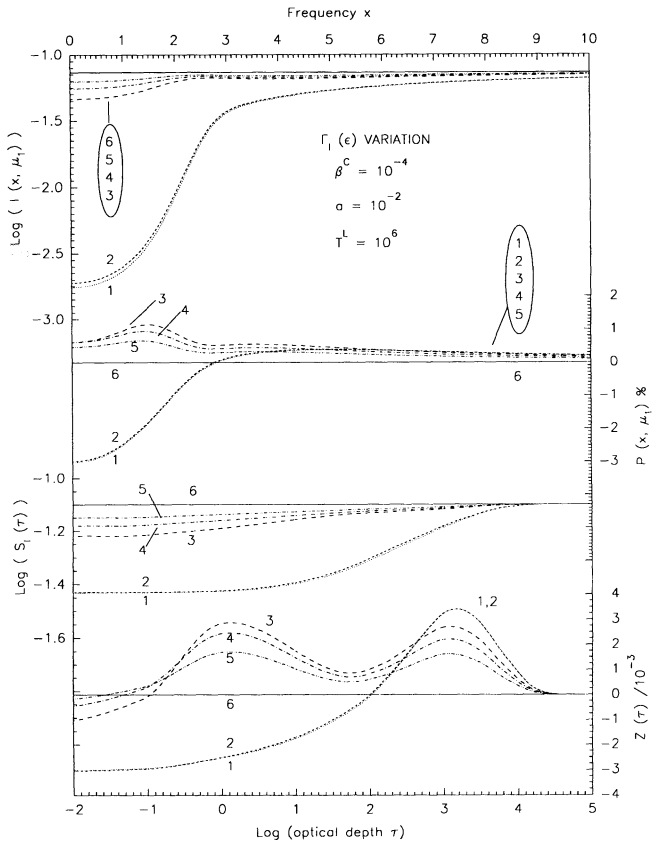

FIG. 3.—Effect of collisions on resonance line polarization. The collisional redistribution is treated exactly, with the Domke–Hubeny (DH) formalism. This figure shows the effect of variation of inelastic quenching collision rate Γ_I on the line intensity and polarization. The models are identified in Table 1 and discussed further in § 3.3.1. The positive peaks in polarization arise due to double-peaked nature of polarization rate $Z(\tau)$ in these highly thermalized models. The following types—dotted (1), medium dashed (2), long dashed (3), dash-dotted (4), dash dot-dotted (5), and thin solid line (6)—in sequence always represent cases (models) (1)–(6), respectively, in every figure, except Fig. 2.

these six models are shown in Table 1. The models are identified by the numbers near the curves. The series of models are analogous to those in which the parameter ϵ is considered as a free parameter in the conventional style (see, e.g., Nagendra 1988). Some more characteristics of the models are shown in the Table 1 and mentioned in § 3.3. The dotted curves correspond to the $\epsilon = 0$ case in which there are no inelastic collisions. Further, as the value of ϵ is increased from 10^{-2} to $\simeq 1$, the inelastic collision rate takes on values in such a way that it is negligible ($\Gamma_I = 2 \times 10^4$ Hz) compared to Γ_R (see curve 1) in the beginning; then becomes as strong ($\Gamma_I = 2 \times 10^8$ Hz) as Γ_R and Γ_C (see curve 4); and finally dominates ($\Gamma_I = 2 \times 10^{12}$ Hz) over Γ_R and Γ_C (see curve 6). Notice that as Γ_I increases the intensity profiles become shallow and weak, and finally when $\epsilon \simeq 1$, namely, when $\Gamma_I = 2 \times 10^{12}$ Hz, almost no line is formed. As Γ_I increases starting from zero, the polarization gradually becomes positive even in the core ($x < 3$), and then decreases until it is almost zero when $\epsilon \simeq 1$. The positive peak polarization is maximum for $\epsilon = \frac{1}{3}$ case (i.e., when $\Lambda_{II} = 0.65$). At the line center, $\epsilon = \frac{1}{2}$ case ($\Gamma_I \simeq \Gamma_R$) gives maximum polarization. As ϵ is increased from 0 to 1, the depth dependence of intensity source function $S_I(\tau)$ gradually becomes weak, and finally for $\epsilon \simeq 1$, as in the LTE case, the source function becomes constant (because our models are isothermal). The polarization rate $Z(\tau)$ however shows interesting variation with optical depth. As ϵ is increased, to values of the order unity, a secondary maxima is formed in $Z(\tau)$ in the optical depth region $\tau \simeq 1$, which is responsible for positive polarization peaks around $x \sim 1.5$. The characteristic depths τ_{FT} in general represent a crossover (see models 1 and 2) from the ϵ-dominated region ($\tau < \tau_{FT}$) in the optical depth space to the β^C-dominated region ($\tau > \tau_{FT}$). From the values of characteristic frequencies x_{PD} of photon destruction (PD) in Table 1 it can be seen that, whereas in models 1 and 2, the parameter β^C controls photon redistribution through multiple scattering random walk, it is inelastic collisions (through destruction and creation of photons during collisional random walk) which dominate in the last four models 3–6. Further, the fact that the collisions come to play an important role even in shallow layers of the atmosphere (as far out as $\tau \sim 1$) explains the polarization for these four models becoming small at the inner core of the line $x < 0.5$ itself. For the same reason, intensity profiles are also shallow (or may even be in emission, when the medium is isothermal and $T^L < 10^4$). Also, polarization becomes generally small throughout the line profile for models 3–6, due to an approach to the LTE situation when the collisions are too strong, compared to other modes of photon de-excitation.

The values of Λ_{II} for models 1–6 are listed in Table 1. It represents the probability that a de-excitation occurs before any elastic collision. The quantity $(1 - \Lambda_{II})$ represents the probability that an elastic collision which does not destroy alignment occurs, followed by a de-excitation of the atom. The equations (44)–(47) give a rough estimate of the relative strength of R_{II-A} type redistribution as compared to R_{III-A} in the exact redistribution matrix. From the table of scaling laws for PRD mechanisms, given in Gayley (1992a), we can see (after identifying Voigt CRD with R_{III-A} for estimates), that for models 3–6 the thermalization depths are very small for Doppler diffusion process which is basically responsible for R_{II-A} redistribution ($\Sigma_{DD} = \tau_{PD}$). Also the "single flight escape frequencies" are well inside the line core $x_{SE}(\Sigma_{DD}) = x_{PD}$. The corresponding quantities for R_{III-A} are even smaller in magnitude (see Gayley 1992a). It is clear from these discussions that the inelastic collisions when $\epsilon \sim 1$ have a strong influence on line formation in the real atmospheres.

3.3.2. *Effect of Variation of Radiative Damping Rate (Γ_R) of the Upper Level*

The total damping parameter a depends on the radiative broadening parameter Γ_R through the equation

$$a = \frac{\Gamma_R + \Gamma_C}{4\pi \Delta\nu_D} . \tag{54}$$

We have parameterized the variation of Γ_R by selecting a series of values for the ratio (Γ_R/Γ_C), holding Γ_C fixed (see Table 2). The values of Γ_I are computed using equation (53). The results are shown in Figure 4. This selection leads to a set of six curves characterized by the parameters shown in Table 2. This series of models differ from those in which the total damping parameter a is considered as a free parameter in the conventional picture, since the collisions specifically play a dominant role in the present series of models. The model parameters other than those mentioned above are listed in § 3.3. The polarization corresponding to curve 1 is almost zero throughout the bandwidth. This happens because of the branching ratios in the Domke–Hubeny redistribution matrix. Since C_4 multiplies the isotropic and noncoherent part of the DH redistribution matrix, there is a complete domination of angularly isotropic (unpolarized) radiation field everywhere in the atmosphere for model 1. The set of branching ratios for model 1 are somewhat unrealistic, but this case represents an extreme situation. The curve 2 also represents a situation similar to that of curve 1. However, the curves 3–6 are represented by the values of radiative and collisional rates which are common in a wide range of astrophysical plasmas. The role of R_{II-A} redistribution becomes important only in models 4–6. Since the damping parameter a undergoes a change of two orders of magnitude, going from model 1 to model 6, Figure 4 also reflects indirectly the effect of

TABLE 2

EFFECT OF VARIATION OF RADIATIVE DAMPING RATE Γ_R[a]

Model	Γ_R (Hz)	Γ_I (Hz)	a	C_1	C_2	C_3	C_4	Λ_{II}	x_{FT}	τ_{FT} ($\times 10^3$)	x_{CS}	T_{opt}
1.....	2×10^5	2×10^1	5.5×10^{-3}	0.0009	0.0001	0.001	0.998	0.001	2.7	3.7	4.2	17.7
2.....	2×10^6	2×10^2	5.6×10^{-3}	0.0089	0.001	0.014	0.976	0.010	2.7	3.7	4.2	17.8
3.....	2×10^7	2×10^3	6.1×10^{-3}	0.0820	0.009	0.106	0.803	0.091	2.8	3.6	4.4	18.3
4.....	2×10^8	2×10^4	1.1×10^{-2}	0.450	0.050	0.203	0.297	0.500	3.2	3.1	5.9	22.3
5.....	2×10^9	2×10^5	6.1×10^{-2}	0.820	0.090	0.049	0.041	0.911	5.0	2.0	14.	39.4
6.....	2×10^{10}	2×10^6	5.5×10^{-1}	0.891	0.099	0.0055	0.0044	0.990	8.6	1.2	42.	82.2

[a] $\Gamma_C = 2 \times 10^8$ Hz, $\Delta\nu_D = 2.9 \times 10^9$ Hz, $D^{(2)} = 0.758 \times 10^8$ Hz, $W_2 = 0.9$, $x_{PD} \equiv x_{FT}$, $\tau_{PD} \equiv \tau_{FT}$, $T_{opt} = (aT^L)^{1/3}$.

variation of a. The characteristic diffusive type variation of R_{II-A} source function $S_I(\tau)$ and anisotropy rate $Z(\tau)$ is clearly seen only in curves 5 and 6, since only these two models represent a dominant contribution of R_{II-A} to the DH redistribution matrix. As shown in Figure 1, the source function $S_I(\tau)$) and anisotropy rate $Z(\tau)$ of R_{III-A} exhibit a variation similar to that of CRD. All the models in Figure 4 are optically and effectively thick [$\epsilon T^L = 10^2$; $(aT^L)^{1/3} \gg 1$] and controlled by continuum absorption parameters β^C. Hence multiple scattering of diffuse radiation field inside the atmosphere plays a crucial role in all these models (it is instructive to contrast them with ϵ-controlled models 3–6 in Fig. 3). As damping parameter a increases, the wings of intensity profiles get highly damped. The polarization profiles also become wide. The crossover point from negative to positive polarization moves out into the wings. The coherent wing point (frequency beyond which R_{II-A} behaves like CS) for model 6 is $x_{CS} = (a/\pi\beta^C)^{1/2} = 42$. For the model 6, the thermalization depth for Doppler diffusion process $\Sigma_{DD}(\tau_{th}) = (1/\epsilon) = 10^4$, and single flight escape frequency $x_{SE}(\Sigma_{PD}) = x_{th} = (a/\epsilon)^{1/3} = 17.7$. Clearly model 6 is dominated by R_{II-A} redistribution, and the frequency diffusion process is controlled by radiative transitions rather than Doppler redistribution. The models shown in Figure 4 have parameters typical of those found in stellar atmospheres. These series of profiles may depict different resonance lines (say, with different a) formed in a given atmospheric model. The overall effect of incresing the radiative broadening rate Γ_R is to increase the width of intensity and polarization profiles. This happens because of an increase in coherence fraction Λ_{II}, or in general, $\bar{\alpha}$ factor (see eqs. [47a] and [33] for meaning of $\bar{\alpha}$).

3.3.3. *Effect of Variation of Elastic Collisional Damping Rate* (Γ_C) *of the Upper Level*

The total damping parameter a depends on the elastic collisional damping rate Γ_C through the equation (54). The quantities Γ_R and Γ_I are held fixed (see Table 3). We have parameterized the variation of Γ_C by selecting a series of values for the ratio (Γ_C/Γ_R). This selection leads to the set of six curves shown in Figure 5. The relevant asymptotic quantities are given in Table 3. The examples of elastic collisions are Van der Waal's broadening of nonhydrogenic lines, mainly by neutral hydrogen and other neutral perturbers. When the perturbers are free charges, then the elastic collisions cause quadratic Stark effect in the radiating nonhydrogenic atoms. However, when the radiators are hydrogenic atoms, and the perturbers are charged, the elastic collisions cause the well-known linear Stark effect in the radiating atoms. The elastic collisions increase the wing opacity at the expense of core opacity through a strong R_{III-A} redistribution component which is basically noncoherent. It is well known that elastic collisions in general

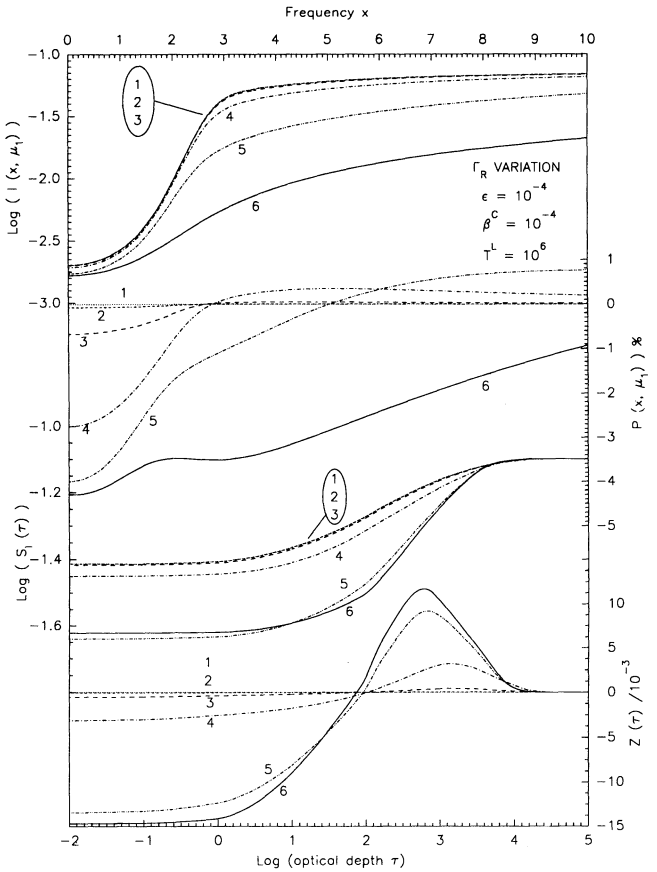

FIG. 4

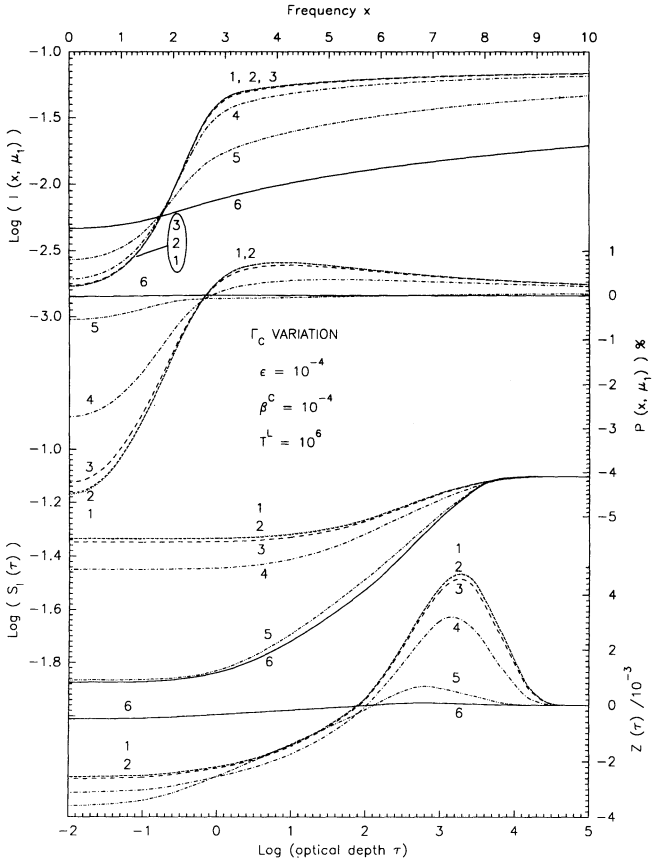

FIG. 5

FIG. 4.—Same as Fig. 3, but now showing the effect of variation of radiative damping rate Γ_R. Highly radiatively damped models show broad shoulders in polarization profile, with no change in sign of polarization. See Table 2 and § 3.3.2 for details.

FIG. 5.—Same as Fig. 3, but now showing the effect of variation of phase changing elastic collision rate Γ_C, on resonance lines. When this kind of collisions are predominant, the line polarization is simultaneously driven toward zero at both the core and wing frequencies. See Table 3 and § 3.3.3 for discussions. Compare with Fig. 4 as well.

TABLE 3

EFFECT OF VARIATION OF ELASTIC COLLISIONAL DAMPING RATE Γ_C[a]

Model	Γ_C (Hz)	$D^{(2)}$ (Hz)	a	C_1	C_2	C_3	C_4	Λ_{II}	x_{FT}	τ_{FT} ($\times 10^3$)	x_{CS}	T_{opt}
1.....	2×10^5	7.6×10^4	5.5×10^{-3}	0.899	0.100	0.0006	0.0004	0.999	2.7	3.7	4.2	17.7
2.....	2×10^6	7.6×10^5	5.6×10^{-3}	0.891	0.100	0.005	0.004	0.991	2.7	3.7	4.2	17.8
3.....	2×10^7	7.6×10^6	6.1×10^{-3}	0.818	0.091	0.049	0.042	0.909	2.8	3.6	4.4	18.3
4.....	2×10^8	7.6×10^7	1.1×10^{-2}	0.450	0.050	0.203	0.297	0.500	3.2	3.1	5.9	22.3
5.....	2×10^9	7.6×10^8	6.1×10^{-2}	0.082	0.009	0.106	0.803	0.091	5.0	2.0	14.	39.4
6.....	2×10^{10}	7.6×10^9	5.5×10^{-1}	0.0089	0.001	0.014	0.976	0.010	8.6	1.2	42.	82.2

[a] $\Gamma_R = 2 \times 10^8$ Hz, $\Gamma_I = 2 \times 10^4$ Hz, $\Delta\nu_D = 2.9 \times 10^9$ Hz, $W_2 = 0.9$, $x_{PD} \equiv x_{FT}$, $\tau_{PD} \equiv \tau_{FT}$, $T_{opt} = (aT^L)^{1/3}$.

cause a destruction of photon correlations (viz., phase of the oscillating atomic dipole) in the atom frame, which results in CRD in atom frame. The branching ratios defined in Domke–Hubeny (1988; see their eqs. [10], [50], and [51]) are slightly modified by Faurobert-Scholl (1992) to include the rate $D^{(2)}$ of elastic collisions that destroy alignment. This is done through a replacement

$$\gamma_e^{c(2)} = \Gamma_I + D^{(2)}, \tag{55}$$

where $\gamma_e^{c(2)}$ (see Domke & Hubeny 1988) is the rate of destruction of electric quadrupole of the level e (in our two-level atom model e is upper level). In other words, it is the total rate of all collisions that change atomic alignment during collisions. In the special case of normal Zeeman triplet ($W_2 = 1$), we get

$$C_4 = \bar{\beta}^{(0)} - \bar{\beta}^{(2)} = \frac{D^{(2)}}{\Gamma_R + \Gamma_I + D^{(2)}}, \tag{56}$$

which is the probability of reemission after an elastic collision that changes alignment (Domke & Hubeny 1988; Faurobert-Scholl 1992). In the case $W_2 \neq 1$, we get the following expressions for the same probability (with $Q_E = \Gamma_C$):

$$C_4 = (\bar{\beta}^{(0)} - W_2\,\bar{\beta}^{(2)}) = (1 - W_2)\,\frac{\Gamma_C}{\Gamma_R + \Gamma_I + \Gamma_C} + W_2\,\frac{D^{(2)}}{\Gamma_R + \Gamma_I + D^{(2)}}. \tag{57}$$

The elastic collision rate $D^{(2)}$ is computed using equation (38), an expression useful when inelastic scattering is weaker, that is, when (Γ_I/Γ_R) is small (see Faurobert-Scholl 1992). This series of models seems to be analogous in the outset to those presented in the previous section (cf. Fig. 4), in the sense that both of them have the same principal parameters (ϵ, β^C, a), but they are different, since the branching ratios in the DH redistribution matrix are completely different from each other. In particular model 6 represents an extreme case, since C_4 multiplies the isotropic and noncoherent part of the DH redistribution matrix, resulting in emergent polarizations being extremely small. The R_{II-A} type redistribution is important only for models 1–4. All the models shown in Figure 5 are optically and effectively thick as well as dominated by continuum absorption. The curves 1–3 are dominated by R_{II-A} redistribution. Curves (5) and 6) are dominated by R_{III-A} redistribution. In Figure 4 as well as Figure 5, the decrease of emergent polarization irrespective of dominance of R_{II-A} or R_{III-A} mechanisms, is associated with an increase of the branching ratio C_4. In Figure 4, as we increased the rate of radiative broadening Γ_R, the intensity and polarization profiles got increasingly broadened, and polarization in particular increased due to an increase in the anisotropy part C_1 of the R_{II-A} redistribution. On the other hand, in Figure 5 the inrease of elastic collision rate Γ_C leads to a broadening of wings of intensity profiles associated with an increase in the intensities of lines for $x < 1.8$. The polarization decreases gradually throughout the profile, with models 1–4 crossing over from negative to positive polarization around $x \sim 2.8$ (see Faurobert-Scholl 1992, Figs. 2 and 3 where similar behavior is seen in a more general case of Ca I 4227 Å line formation in a realistic solar atmosphere model). This behavior of polarization profiles is due to uniform increase of C_4 as we go from model 1 to model 6. The coefficient C_1 also decreases uniformly. However C_3 increases going from model 1 to model 4 where $\Gamma_C = \Gamma_R$, and decreases again to $\sim 10^{-2}$ in model 6. Thus, the fall in anisotropy of R_{III-A} redistribution which controls models 5 and 6 is responsible for polarization approaching zero all over the line. Indeed it is expected that the R_{II-A} scaling laws that we have used everywhere cannot be exact in situations where R_{III-A} is fully dominant. We have always used R_{II-A} scaling laws mainly because, for the parameteric range we are concerned with, the characteristic frequencies are generally closer to line core and $x_{PD} = x_{FT}$, excepting a few models. In Figure 4 the crossover frequency point of polarization moved away from line center as Γ_R was increased. By now, the crossover point remains nearly the same in spite of an increase in damping parameter a, perhaps due to a constant value of Γ_R, for models shown in Figure 5. The overall effect of increase in the rate Γ_C of phase changing elastic collisional broadening, is to make the intensity profiles shallow and the polarization tend to zero, across the bandwidth of the line. This happens because of an increase in noncoherence fraction $(1 - \Lambda_{II})$, or in general $\bar{\beta}^{(0)}$ factor (see eqs. [47b] and [34] for the meaning of $\bar{\beta}^{(0)}$ factor).

3.3.4. *Effect of Variation of Alignment Destroying Elastic Collisional Damping Rate* ($D^{(2)}$)

The branching parameter $\bar{\beta}^{(2)}$ depends explictly on the alignment destroying elastic collision rate $D^{(2)}$. We have parameterized the variation of $D^{(2)}$ by selecting a series of values for $(D^{(2)}/\Gamma_C)$. The results are presented in Figure 6 and Table 4. As $D^{(2)}$ is increased, the constant C_3 decreases and C_4 increases, both of which lead to a gradual decrease of polarization in the line core. As already mentioned earlier, C_4 represents in our models the probability that an alignment destroying elastic collision occurs followed by a de-excitation of the atom. The factor C_3 represents the probability that a purely phase changing elastic collision occurs followed by

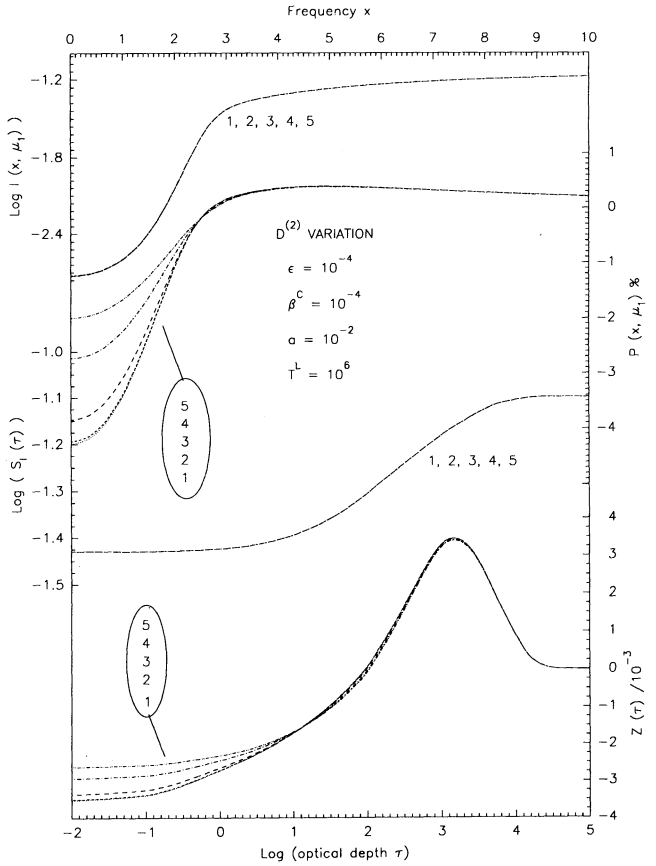

FIG. 6.—Same as Fig. 3, but now showing the effect of alignment changing elastic collision rate $D^{(2)}$ on resonance lines. This mechanism affects only the anisotropy fraction of the scattering. Compare also with Fig. 5. The details of the models are shown in Table 4 and discussed in § 3.3.4.

a reemission. However, the relative strength of these two processes dictates the final state of the radiating atom. Notice that the coherence fraction Λ_{II} remains constant. Therefore the contributions of R_{II-A} and R_{III-A} are nearly equal and the same for all the five models. It is important to note that although $D^{(2)}$ is changed by four orders of magnitude, the changes in the intensity profile is negligible, and only polarization profile is sensitive to changes in $D^{(2)}$ (see Faurobert-Scholl 1992 also). The increase of $D^{(2)}$ factor neither broadens the intensity profiles nor makes them shallow, unlike inelastic collision rate Γ_I which, apart from destroying alignment of atoms, destroys the photons, thereby causing strong changes in the intensity profile, particularly when Γ_I exceeds other radiative and collisional rates. The alignment changing elastic collisions represented by $D^{(2)}$ can thus be seen purely as polarization destroying (or depolarizing) kind of collisions. They affect the polarization by destroying phase relations and causing a simultaneous reduction of anisotropic scattering (C_3), and enhancement of isotropic scattering (C_4) in the redistribution process. In normal stellar atmospheric conditions we have $\Gamma_I < (\Gamma_C, D^{(2)})$. Thus the polarization profile can provide a better diagnostic of elastic-type collisional perturbations (although it is difficult to distinguish, in the line core region, the role of Γ_C from that of $D^{(2)}$), than the scalar intensity alone. The important difference between the effect of Γ_C and $D^{(2)}$ on polarization is that the former affects intensity profile and the polarization profile over a large bandwidth, while the latter manifests itself only through polarization changes in a narrow bandwidth $x \leq 3$. In reality both the upper and lower levels are broadened by collisions in general, which makes it mandatory to invoke a combination of R_{V-A} and R_{III-A} type redistribution functions in the exact DH redistribution matrix. The overall effect of $D^{(2)}$ parameter is thus to depolarize the line irrespective of the type of redistribution or the level structure of the transition under

TABLE 4

EFFECT OF VARIATION OF ELASTIC COLLISIONAL DAMPING RATE $D^{(2)}$ [a]

Model	r	$D^{(2)}$ (Hz)	C_1	C_2	C_3	C_4	Λ_{II}
1.....	0.001	1.6×10^5	0.499	0.055	0.401	0.045	0.554
2.....	0.010	1.6×10^6	0.499	0.055	0.394	0.058	0.554
3.....	0.100	1.6×10^7	0.499	0.055	0.334	0.112	0.554
4.....	0.500	0.8×10^8	0.499	0.055	0.143	0.303	0.554
5.....	1.000	1.6×10^8	0.499	0.055	0.000	0.446	0.554

[a] $\Gamma_R = 2 \times 10^8$ Hz, $\Gamma_I = 2 \times 10^4$ Hz, $\Gamma_C = 1.61 \times 10^8$ Hz, $\Delta\nu_D = 2.9 \times 10^9$ Hz, $W_2 = 0.9$, $x_{PD} \equiv x_{FT}$, $\tau_{PD} \equiv \tau_{FT}$, $x_{FT} = 3.2$, $\tau_{FT} = 3.2 \times 10^3$, $x_{CS} = 5.64$, $r = D^{(2)}/\Gamma_C$.

TABLE 5

EFFECT OF VARIATION OF DEPOLARIZATION FACTOR $(1 - W_2)$[a]

Model	W_2	C_1	C_2	C_3	C_4	Λ_{II}
1.....	0.000	0.000	0.554	0.000	0.446	0.554
2.....	0.333	0.185	0.369	0.071	0.375	0.554
3.....	0.500	0.277	0.277	0.106	0.340	0.554
4.....	0.667	0.369	0.185	0.142	0.304	0.554
5.....	1.000	0.554	0.000	0.212	0.234	0.554

[a] $\Gamma_R = 2 \times 10^8$ Hz, $\Gamma_I = 2 \times 10^4$ Hz, $\Gamma_C = 1.61 \times 10^8$ Hz, $\Delta\nu_D = 2.9 \times 10^9$ Hz, $D^{(2)} = 0.61 \times 10^8$ Hz, $x_{PD} \equiv x_{FT}$, $\tau_{PD} \equiv \tau_{FT}$, $x_{FT} = 3.2$, $\tau_{FT} = 3.2 \times 10^3$, $x_{CS} = 5.64$.

consideration. Faurobert-Scholl (1993) has shown that the collisional depolarization alone cannot fit the observed polarization of solar Sr I 4607 Å line, and an additional weak field Hanle depolarization in the photosphere of the Sun is necessary. Although it is difficult to extend that analogy to stellar photospheric polarized line formation, it is apparent that the role of collisional redistribution cannot be ignored when modeling a high spectral resolution polarimetric data that may be available in future, which can possibly distinguish the role of major line broadening mechanisms. It is also important to recognize that in a certain region of parameter space [namely, $(\Gamma_C, D^{(2)}) < \Gamma_R$], both Γ_C and $D^{(2)}$ (say, due to van der Waal's type interaction) strongly affect only polarization in the core and leave the intensity profile unaffected. This situation is realizable in reality, and has important diagnostic potential.

3.3.5. *Effect of Variation of Level Depolarization Factor* (W_2)

The factor W_2 is the probability that intrinsic level depolarization does not occur. It is the same as the factor E_1 in the Rayleigh phase matrix for dipole scattering of resonance line photons by atoms (see Chandrasekhar 1960). W_2 depends purely on the level configuration of the transition under consideration. For a strong resonance line arising in a $(j_u = 1 \rightarrow j_l = 0)$ type of transition, $W_2 = 1$. But, for a subordinate line, such as for an example due to a $(j_u = 5/2 \rightarrow j_l = 3/2)$ type of transition, $W_2 = 0.53$. We have parameterized the variation of this intrinsic depolarization factor W_2 by taking a series of values for W_2 in the range (0, 1) as shown in Table 5. The results are shown in Figure 7. For an $s - p - s$ transition in a normal Zeeman triplet there is no intrinsic

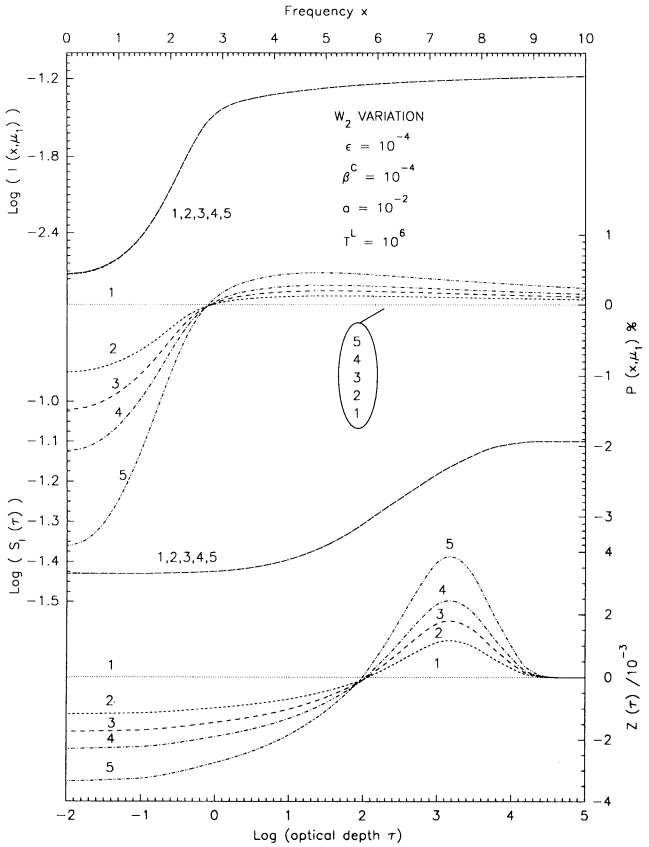

FIG. 7.—Same as Fig. 3, but now showing the effect of variation of atomic level depolarization factor $(1 - W_2)$ on resonance lines. Mainly the line polarization is affected. When $W_2 = 0$, the polarization is equal to zero in the line. Compare with Fig. 6 also. The details of the models are given in Table 5 and discussed further in § 3.3.5.

depolarization ($W_2 = 1$). The choise $W_2 = 0$ case represents complete depolarization (no polarization) and other intermediate values represent partial intrinsic depolarization. The importance of this atomic depolarizability ($1 - W_2$) on emergent polarization, as compared to the collisional redistribution, can be gauged by observing the way in which it strongly couples the various branching ratios. For example, in the C_4 factor, there is a branching between phase-changing elastic collisions weighted by ($1 - W_2$) and the alignment changing elastic collisions by W_2. From Figure 7 we can see that the variation of W_2 causes negligible change in the intensity of the profile. In this respect the effect of variation of W_2 on intensity profile is quite similar to that of $D^{(2)}$. Notice that although the coherence fraction Λ_{II} is the same in both these sets of models, the behavior of emergent polarization is somewhat different. Variation of W_2 affects the polarization in the line core as well as wings and affects the collisional branching ratio for coherent and noncoherent process in a rather symmetric manner. As we go from $W_2 = 0$ to $W_2 = 1$, the polarization in the entire line increases. The crossover point from negative to positive polarization (at $x \sim 2.8$) is not affected however. Each profile in Figure 7 can depict a different line with different level depolarizability. The overall effect of W_2 is to change the polarization by affecting the angular anisotropy of the local radiation field, irrespective of the kind of frequency redistribution and collisional redistribution that control the line formation.

3.3.6. *Effect of Variation of Doppler Width ($\Delta\nu_D$) of the Line*

The Doppler width $\Delta\nu_D$ depends on line center frequency ν_0, temperature T_e, and mass M^a of the radiator. We have parameterized the variation of $\Delta\nu_D$ purely by selecting a set of values for M^a and keeping ν_0 and T_e constant (isothermal medium). The values of M^a correspond roughly to the atomic weights of Sr, Ca, Mg, He, and H, respectively. The rest of the model parameters are shown in Figure 8 and Table 6. The branching ratios of all the models are identical. The R_{II-A} redistribution with anisotropic scattering (through the factor C_1) dominates the coherence fraction Λ_{II}, which remains at a constant value of 0.5, meaning equal contributions from both R_{II-A} and R_{III-A} redistribution mechanisms. As the Doppler width $\Delta\nu_D$ decreases, the damping parameter a increases. This results in the broadening of intensity profiles, for frequencies $x > 2.2$. The profiles are well resolved only in the intermediate ($2.2 < x < 10$) frequency band. The polarization profiles show a somewhat unusual behavior. For core frequencies $x < 2.2$, decrease of Doppler width causes a decrease in the magnitude of polarization. For frequencies $x > 6$, a reversal of this behavior is seen. In the intermediate frequency bandwidth ($2.2 < x < 6.0$) the polarization curves successively change over their frequency dependence relative to each other. This is essentially due to the variation in the location of the frequency region which separates CRD-dominated core and coherent scattering-dominated far wings (see x_{CS} in Table 6), when Doppler width is changed as a model parameter. The source function $S_I(\tau)$ for all the models reach the same equilibrium value for $\tau > \tau_{th}(x_{th}) = 10^4$. As the Doppler width decreases, the source function $S_I(\tau)$ uniformly decreases for $\tau < \tau_{th}(x_{th})$ and the polarization rate $Z(\tau)$ uniformly increases for $\tau < T^C = 10^2$. The polarization rate also shows same behavior for $\tau > 10^2$. This behavior of line core ($x < 3$) polarization uniformly decreasing in magnitude in spite of polarization rate $Z(\tau)$ increasing uniformly in the relevant range of optical depths $\tau < 10^2$ is peculiar to the cases in which the damping parameter a is increased uniformly keeping all other collisional and radiative parameters constant. It is basically due to the fact that we force the emergent line core intensity to increase, through increased photon escape [see $S_I(\tau)$ curves], but the corresponding source function for Stokes Q parameter $S_Q(\tau)$ increases only weakly in $\tau < 10^2$, for an increase in the damping parameter a in the above said manner. Thus the emergent degree of polarization (Q/I) decreases in the core, although the emergent Q Stokes parameter shows a small increase in magnitude as we increase the damping parameter a. Notice that a similar behavior is seen in Figure 5 also, but the reason for such a behavior there, is the strong decrease of coherence fraction Λ_{II} when Γ_C was increased. The effect of variation of a on the frequency thermalization and Doppler diffusion is discussed briefly in earlier sections. The overall effect of decreasing the Doppler width $\Delta\nu_D$ uniformly is to broaden the wings of intensity absorption profiles at the expense of the core, and to increase the polarization only in the far wings. The profiles 1–5 shown in Figure 8 may depict the resonance lines of different elements emitted at same wavelength $\lambda_0 = 500$ Å. But the $1/(M^a)^{1/2}$ dependence of Doppler width on atomic mass makes this effect of $\Delta\nu_D$ rather weak, when compared to the changes caused by radiative and collisional rates.

3.4. *Effect of Electron Scattering on the Wing Polarization in Resonance and Subordinate Lines*

In this section we study the near wing collisional redistribution in the presence of electron scattering in the atmosphere. For this purpose we selected the parameterized models representing collisions, as in § 3.2. The results are presented in Figure 9 and Table 7. Our choice of β^e value corresponds to an electron scattering optical depth of $T^e = \beta^e T^L = 10^4$ which results in a large thermalization of photons by this process. Mihalas, Kunasz, & Hummer (1976) have studied the PRD line formation in SS atmospheres including electron scattering, in the presence of a strong continuum. In that paper the authors have shown that the so-called complete frequency redistribution in electron scattering (CRES) is a good approximation, to the exact electron partial redistribution

TABLE 6

EFFECT OF VARIATION OF DOPPLER BROADENING RATE $\Delta\nu_D$[a]

Model	r	$\Delta\nu_D$ ($\times 10^9$ Hz)	a	C_1	C_2	C_3	C_4	A_{II}	x_{FT}	τ_{FT} ($\times 10^3$)	x_{CS}	T_{opt}
1.....	0.025	18	1.8×10^{-3}	0.45	0.05	0.2	0.3	0.5	2.1	4.9	2.4	12.1
2.....	0.100	9	3.5×10^{-3}	0.45	0.05	0.2	0.3	0.5	2.4	4.1	3.3	15.2
3.....	0.500	4	7.8×10^{-3}	0.45	0.05	0.2	0.3	0.5	3.0	3.4	5.0	19.9
4.....	1.000	3	1.1×10^{-2}	0.45	0.05	0.2	0.3	0.5	3.2	3.1	5.9	22.3
5.....	2.000	2	1.6×10^{-2}	0.45	0.05	0.2	0.3	0.5	3.5	2.9	7.1	25.0

[a] $\Gamma_R = 2 \times 10^8$ Hz, $\Gamma_C = 2 \times 10^8$ Hz, $\Gamma_I = 2 \times 10^4$ Hz, $D^{(2)} = 0.758 \times 10^8$ Hz, $W_2 = 0.9$, $\lambda_0 = 5000$ Å, $x_{PD} \equiv x_{FT}$, $\tau_{PD} \equiv \tau_{FT}$, $T_{opt} = (aT^L)^{1/3}$, $r = (M^a/M^a_{ref})$, $M^a_{ref} = 40$ amu, $T_e = 5000$ K.

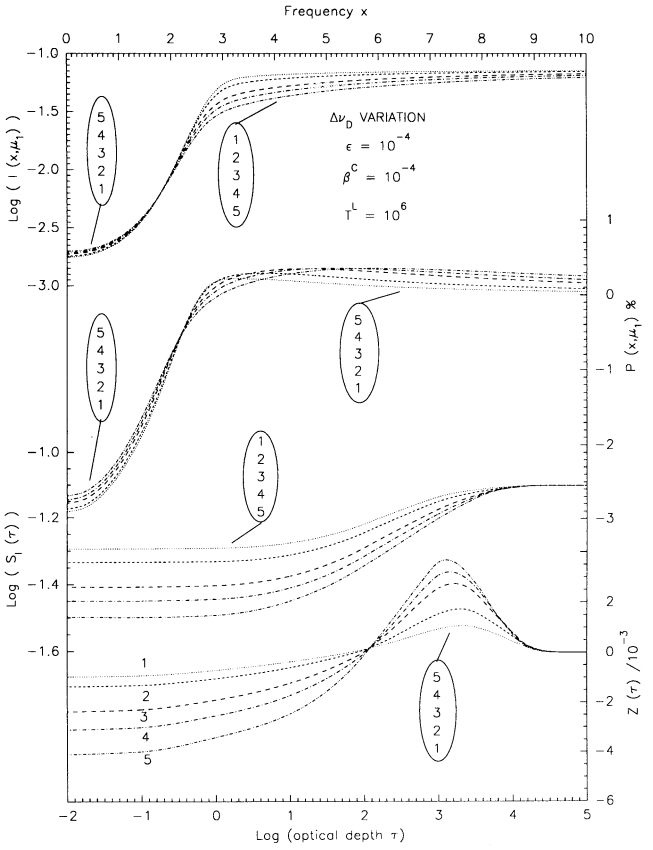

FIG. 8

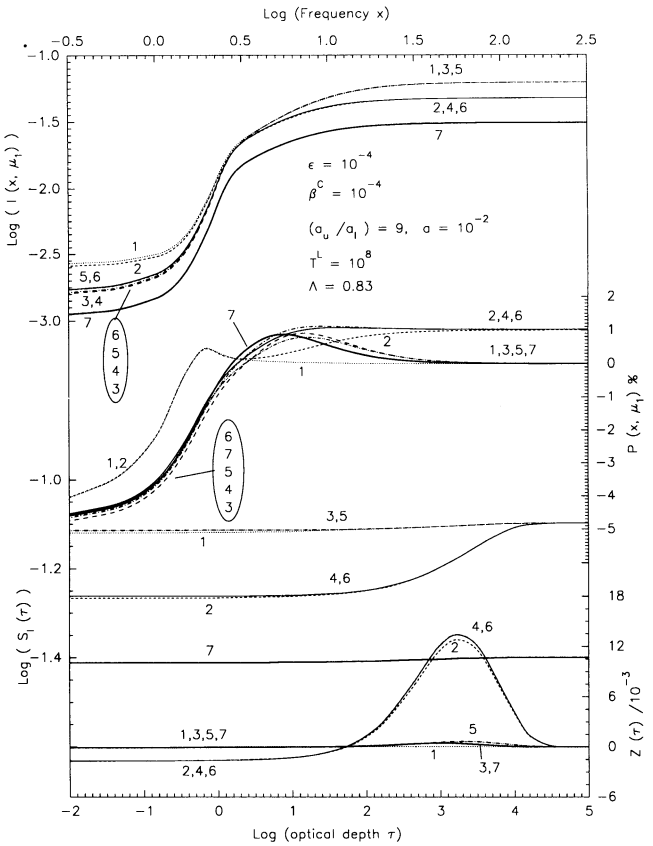

FIG. 9

FIG. 8.—Same as Fig. 3, but now showing the effect of variation of Doppler width $\Delta\nu_D$ of the line. The models could depict the lines of different elements formed in the same isothermal spherical shells. See Table 6 and § 3.3.6 for discussion. Also compare with Figs. 4 and 5.

FIG. 9.—Effect of electron scattering on line polarization in spherical atmospheres. The collisional redistribution is included through a linear combination of redistribution functions, in a parameterized way ($\Lambda = 0.83$) as in the case of Fig. 2. Model 7 is represented by thick solid line. Electron scattering in general leads to a constant polarization of $\sim 1\%$ in the line wings, for $\beta^e = 10^{-4}$ models, as compared to negligible wing polarization in models where electron scattering is neglected ($\beta^e = 0$). See Table 7 and § 3.4 for details.

function, and provides a practical way of including electron scattering when $\beta^e \leq \beta^C$ in transfer computations. Hence we have employed only CRES in our computations to represent noncoherent electron scattering. The approximation involved in the use of CRES is that the electron Doppler width is so large that the electron scattering contribution is dominated by the local mean intensity compared to diffuse scattering on electrons. The CRES is better than other limiting forms, namely CES, and is simpler than the use of appropriate redistribution function (see Mihalas et al. 1976). The curves 1 and 2 represent the CRD line formation with $\beta^e = 0$ and 10^{-4}, respectively. The CRES approximation is employed for electron scattering redistribution function. The curves 1 and 2 show the impact of electron scattering on a resonance line. Since we have selected the branching ratio of $\Lambda = 0.83$ in equation (22), the line is not dominated by collisional redistribution.

The electron scattering does not allow the line wing photons to easily thermalize to the continuum level and completely redistributes the line photons over a large frequency bandwidth and over several mean free paths in the atmosphere, leading to easier

TABLE 7

EFFECTS OF ELECTRON SCATTERING AND COLLISIONAL REDISTRIBUTION[a]

Model	$R^a(x, x')$	$R^e(x, x')$	β^e	β	x_{FT}	τ_{FT} ($\times 10^3$)	x_{CS}
1.....	CRD	0	0	10^{-4}	4.2	2.4	9.8
2.....	CRD	CRES	10^{-4}	2×10^{-4}	3.5	1.4	6.9
3.....	$R_{II,III}$	0	0	10^{-4}	4.2	2.4	9.8
4.....	$R_{II,III}$	CRES	10^{-4}	2×10^{-4}	3.5	1.4	6.9
5.....	$R_{V,III}$	0	0	10^{-4}	4.2	2.4	9.8
6.....	$R_{V,III}$	CRES	10^{-4}	2×10^{-4}	3.5	1.4	6.9
7.....	$R_{II,III}$	0	10^{-4}	2×10^{-4}	3.5	1.4	6.9

[a] $W_2 = 0.9$, $\Lambda = 0.83$, $\beta = \beta^C + \beta^e$, $a_u = 2.7 \times 10^{-2}$, $a_l = 0.3 \times 10^{-2}$, $a = a_u + a_l$, $x_{PD} \equiv x_{FT}$, $\tau_{PD} \equiv \tau_{FT}$, $T_{eff} = 10^2$, $T^C = (10^4, 2 \times 10^4)$, $T_{opt} = 144$.

escape of photons. Hence the source functions $S_I(\tau)$ for $\beta^e = 10^{-4}$ falls drastically below the $S_I(\tau)$ of regular ($\beta^e = 0$) cases for optical depths $\tau < 10^4$, resulting in the overall weakening of the line in the entire bandwidth. Further, the far wing ($x > 100$) intensity profiles develop broad shoulders. Due to overriding influence of electron scattering on line formation, the identities of individual atomic redistribution processes involved are completely lost, and all of them saturate to a constant positive polarization of $\sim 1\%$. A similar behavior is seen in the intensity profiles also [see the pairs of curves (1, 2), (3, 4), and (5, 6)]. The pair of curves (3, 4) show the effect of electron scattering on a resonance line when collisions are included. Similarly the pair of curves (5, 6) refer to subordinate lines. Notice that the polarization curves of all these cases clearly show the gradual transition from dominance of atomic redistribution in the line core to the dominance of electron scattering over the rest of the frequency bandwidth. The number of times a typical line photon can be scattered by electrons before it is absorbed by the continuum in the very far wings ($x > 100$) is given by $[(\beta^C + \beta^e)/(\beta^C)]$, which is equal to 2.0 in our case. The electron scattering can also be considered as a random walk in the spherical shell with a mean free path given by $1/[\chi^C(r) + \chi^e(r)]$. In a spherical medium, it becomes an outward biased (to larger radius) random walk, although the bias is quite small in our models since R is small and T^L is large. The presence of an atomic continuum absorption β^C acts as a moderator to the electron redistribution by limiting the number of electron scatterings. The main effect of electron scattering on polarization is that it reaches a nearly constant (frequency independent) value of $\simeq 1\%$ extending up to very far on the wings. Curve 7 shows the case where the electron scattering opacity represented by β^e is treated as just another source of isotropic continuum absorption, and arithmetically added on to β^C as is normally done. The intensity absorption profile deepens further (compare to curve 3) at all the frequency points in general, and the degree of polarization decreases in magnitude throughout the profile, as also reaching the zero polarization level faster than the case where $\beta^e = 0$. Thus it is not advisable to add the electron scattering opacity to the atomic continuum opacity as just a source of opacity in accurate modeling of observed line profiles.

Note that we can recover our expression for total source function (see § 2) from the expressions given in Hubeny (1985a; his eqs. [40] and [41]), by a replacement $\beta^C \rightarrow \beta^C + \beta^e$. Hence all the expressions derived in that paper for PRD transfer in the line can generally be used as a first approximation, for cases including noncoherent electron scattering also, However, this replacement implies that electron scattering is treated only as scattering part of the continuum source function whose thermal emission part is the frequency-independent Planck function B. Thus our new defintion of the condition for importance of PRD effects now reads $(\beta^C + \beta^e) \ll (a/\pi^2)$, instead of the usual $\beta^C \ll (a/\pi^2)$ when electron scattering was neglected. While this replacement $\beta^C \rightarrow (\beta^C + \beta^e)$ is exact when electron redistribution is a purely coherent type (CES), it is only a numerical approximation for electron complete redistribution (CRDE). During CES the frequency correlation of line photons are not effectively destroyed, which is not the case with CRES mechanism.

4. CONCLUSIONS

The main conclusions of our computations are as follows: polarization profiles provide a sensitive diagnostic of different types of collisions that affect the line formation. The line core polarization is as useful as the wing polarization for the purpose of diagnosis. It is also seen that the scaling laws and the asymptotic expressions derived for scalar transfer theory are very useful in the interpretation and understanding of polarization results. The positive polarization maxima near the line core, for the models considered here, can provide an estimate of the critical frequency point for wing thermalization in situations where a considerable amount of wing coherence exists, which is practically the case with resonance lines. In the exact treatment of collisional redistribution according to the Domke–Hubeny redistribution matrix, it is possible in principle to differentiate more accurately the elastic and inelastic (Γ_I) collisional effects, if we so require. This point is very useful in theoretical modeling of resonance lines in stellar atmospheres, if elastic and inelastic collisions are dominated by different kinds of perturbers (like in the cases presented in this paper, where the elastic collisions are mostly those with neutral hydrogen atoms, while the inelastic ones are those with free electrons). Unlike other collisional rates, only the pure radiative rate (Γ_R) leads to a broadening of the intensity and polarization profiles, in the conventional sense of line broadening. The phase-changing collisions (Γ_C) and alignment-changing collisions ($D^{(2)}$), on the other hand, cause what can be generally called collisional depolarization, although the later can affect only the polarization profile and not the intensity profile. The intrinsic level depolarization ($1 - W_2$) caused by the nature of the atomic transition considered should be included as a basic atomic data in modeling line polarization profiles. The rather weak dependence of polarization on the variation of Doppler width through existing temperature structure or otherwise, is advantageous from the modeling point of view. The sensitivity of polarization to the various branching ratios also shows the need to compute them accurately. Although electron scattering leaves the atomic redistribution effects (including even collisions) somewhat unaltered in the line core, it completely dominates the far line wing polarization, in our models (which have a strong continuum absorption). Thus the general effect of electron scattering is to increase and maintain a constant level of linear polarization up to frequencies very far in the wings, in spite of an increased photon escape caused by itself. A variety of physical processes whose role is yet to be established affect the frequency redistribution in general, and polarization in particular (see Hubeny 1985b for an illuminating discussion of many physical effects that are yet to be included in an ideal frequency redistribution model, not to speak of multilevel effects, realistic atmospheric models, etc.). The results shown in this paper conform to what is classified as "standard PRD problem under nonstandard conditions" by Hubeny (1985b, p. 53).

I am grateful to I. Hubeny, for his critical remarks and suggestions which helped me to improve the paper a great deal. I am grateful to M. Faurobert-Scholl for useful information regarding Domke–Hubeny redistribution functions. I am grateful to B. A. Varghese and R. Surendiranath for their help regarding figures.

REFERENCES

Adams, J. F. 1972, ApJ, 174, 439
Ballagh, R. J., & Cooper, J. 1977, ApJ, 213, 479
Chandrasekhar, S. 1960, Radiative Transfer (New York: Dover)
Domke, H., & Hubeny, I. 1988, ApJ, 334, 527
Faurobert-Scholl, M. 1987, A&A, 178, 269
———. 1988, A&A, 194, 268
———. 1991, A&A, 246, 469
———. 1992, A&A, 258, 521
———. 1993, A&A, 268, 765
Frisch, H. 1980, A&A, 83, 166
Gayley, K. G. 1992a, ApJS, 78, 549
———. 1992b, ApJ, 390, 573
———. 1992c, ApJ, 390, 583
Heinzel, P. 1981, JQSRT, 25, 483
Heinzel, P., & Hubeny, I. 1982, JQSRT, 27, 1
———. 1983, JQSRT, 30, 77
Hubeny, I. 1985a, A&A, 145, 463
———. 1985b, in Progress in Stellar Spectral Line Formation Theory, ed. J. E. Beckman & L. Crivellari, NATO ASI Series C152 (Dordrecht: Reidel), 27
Hubeny, I., & Cooper, J. 1986, ApJ, 305, 852
Hubeny, I., & Heinzel, P. 1984, JQSRT, 32, 159
Hummer, D. G. 1962, MNRAS, 125, 21
Kunasz, P. B., & Hummer, D. G. 1974, MNRAS, 166, 19
Landi degl'Innocenti, E., Bommier, V., & Sahal-Brechot, S. 1990, A&A, 235, 459
Matta, F., & Reichel, A. 1971, Math. Comput., 25, 339
McKenna, S. J. 1984, Ap&SS, 106, 283
———. 1985, Ap&SS, 108, 31
Mihalas, D. 1978, Stellar Atmospheres (San Francisco: Freeman)
Mihalas, D., Kunasz, P. B., & Hummer, D. G. 1975, ApJ, 202, 465
———. 1976, ApJ, 210, 419
Mohan Rao, D., & Rangarajan, K. E. 1993, A&A, 274, 993
Nagendra, K. N. 1988, ApJ, 335, 269
———. 1989, Ap&SS, 154, 119
Omont, A., Smith, E. W., & Cooper, J. 1972, ApJ, 175, 185
Rees, D. E. 1978, PASJ, 30, 455
Rees, D. E., & Murphy, G. A. 1987, in Numerical Radiative Transfer, ed. W. Kalkofen (New York: Cambridge Univ. Press), 241
Rees, D. E., & Saliba, G. J. 1982, A&A, 115, 1
Saliba, G. J. 1985, Sol. Phys., 98, 1
Stenflo, J. O., Baur, T. G., & Elmore, D. F. 1980, A&A, 84, 60
Streater, A., Cooper, J., & Rees, D. E. 1988, ApJ, 335, 503